MULTI-MODALITY EXPERIMENTAL APPROACH IN ORTHOPEDIC BIOMECHANICS WITH CLINICAL & DEVICE APPLICATIONS

A Thesis

by

ZACHARY TODD LAWSON

Submitted to the Graduate and Professional School of
Texas A&M University
in partial fulfillment of the requirements for the degree of

MASTER OF SCIENCE

Chair of Committee,	Michael R. Moreno
Committee Members,	John C. Criscione
	Abhishek Jain
	Harry Hogan
Head of Department,	Mike McShane

Dec 2021

Major Subject: Biomedical Engineering

ABSTRACT

Orthopedic biomechanics is the field of study wherein the principles of mechanics are applied to biological problems in the characterization, evaluation, and repair of the musculoskeletal system (Mow, et al. 2005). Repair methods, such as orthopedic devices and surgical interventions, are often evaluated through in vitro mechanical testing. Because of the complex loading environment in the human body, relevant tests can be difficult to design. In light of these challenges, the present work surveys three biomechanical experiments developed and performed with clinical orthopedic surgical practice or device development. First, a novel double tension slide technique for surgical repair of distal bicep tendon rupture is mechanically evaluated. Second, a novel method is developed for mechanically evaluating cranial defect repair in small animals with direct application for a novel shape memory polymer repair device. Third, novel femoral broach designs are mechanically evaluated for cutting efficiency with application in improved femoral subsidence for total hip replacement patients.

DEDICATION

To my wife, Ada, and to our son, Benjamín

CONTRIBUTORS AND FUNDING SOURCES

Contributors

This work was supported by a thesis committee consisting of Professors Michael R. Moreno (chair), John C. Criscione, and Abhishek Jain of the Department of Biomedical Engineering and Professor Harry Hogan of the Department of Mechanical Engineering.

The surgical technique in Chapter 2 was developed, designed, described, and performed by Dr. Patrick McCulloch, Kyle Sochacki, and Robert A. Jack II of Houston Methodist Research Hospital. The description is taken from the 2020 publication Sochacki, K. R., Jack, R. A., Lawson, Z. T., Dong, D., Robbins, A. B., Moreno, M. R., & McCulloch, P. C. (2020). Distal Biceps Tendon Repair Using a Double Tension Slide Technique. Arthroscopy techniques, 9(5), e683-e689 and the 2021 publication Sochacki, K. R., Lawson, Z. T., Jack, R. A., Dong, D., Robbins, A. B., Moreno, M. R., & McCulloch, P. (2021). Double Tension Slide Technique as a Novel Repair for Distal Biceps Tendon Tear: A Biomechanical Evaluation. Cureus, 13(3).

The design of the push-out testing method and fixtures in Chapter 3 was a collaborative effort with Jiwan Han in the Dept. of Mechanical Engineering. This was published in 2021 in Lawson, Z. T., Han, J., Saunders, W. B., Grunlan, M. A., Moreno, M. R., & Robbins, A. B. (2021). Methodology for Performing Biomechanical Push-Out Tests for Evaluating the Osseointegration of Calvarial Defect Repair in Small Animal Models. MethodsX, 101541. and in Pfau, M. R., Beltran, F. O., Woodard, L. N., Dobson, L. K., Gasson, S. B., Robbins, A., Lawson, Z.T., ... & Grunlan, M. A. (2021). Evaluation of a Self-Fitting, Shape Memory Polymer Scaffold in a Rabbit Calvarial Defect Model. Acta Biomaterialia.

The testing materials (i.e., broaches and SawBones blocks) for Chapter 4 were provided by Chris Sidebotham from Biomedtrix, Inc. The clinical background was largely provided by Dr. W. Brian Saunders of the Dept. of Small Animal Clinical Sciences.

All other work conducted for the thesis was completed by the student independently.

Funding Sources

Funding for the work in Chapter 2 was provided by Houston Methodist Research Hospital.

Funding for the work in Chapter 3 was provided by NIH NIDCR 1R01DE025886-01A1.

Funding for the work in Chapter 4 was provided by the Dept. of Small Animal Clinical Sciences via the GINN grant program.

TABLE OF CONTENTS

Page

LIST OF FIGURES

FIGURE Page

LIST OF TABLES

TABLE Page

1. INTRODUCTION

Orthopedic biomechanics is the field of study wherein the principles of mechanics are applied to biological problems that usually arise in the characterization, evaluation, and repair of the musculoskeletal system. [2] Repair methods, such as orthopedic devices and surgical interventions, are often evaluated through *in vitro* mechanical testing. Because of the complex loading environment in the human body, relevant mechanical tests can be difficult to design; in particular, there are conceptual difficulties identifying the relevant testing modality (e.g. uniaxial tension, four point bend, cantilever bending, etc) and technical difficulties in implementing non-standard physiological loading scenarios on standard testing machines. [2, 3] One approach is to modify standard testing machines with custom fixturing to accommodate physiological loading; however, this approach is highly labor intensive, expensive, and study-specific. A second approach is to use a custom testing system (e.g., simVITRO systems), designed to replicate specific physiological loading; however, while these systems can precisely replicate physiological loading, they are often cost prohibitive and have an exceedingly narrow functional use. For example, the popular simVITRO system from The Cleveland Clinic Foundation has a price point in excess of $300,000 for the base system with additional modules to replicate specific joint motion (e.g. hip, wrist, spine, etc) priced at $5,000 each. Unsatisfied with these approaches, the Biomechanical Environments Laboratory (BMEL) developed an in-house reconfigurable testing machine (R.T.S.) designed to meet the above needs and to open up the possibility space for more complex orthopedic biomechanical projects at the much lower price point of $50,000. [3] With the first iteration of this testing system designed and built, the present work builds on this foundation by leveraging the system in the design and execution of experiments with application in orthopedic biomechanics. Herein, three mechanical experiments of various testing modalities are developed and performed. Each experiment is self contained, having direct application for a specific orthopedic biomechanical question with application either in surgical practice or device design; these are the primary takeaways of this work. Taken together, the various experiments secondarily serve to demonstrate the versatility in the re-

configurable machine's application. This work represents a stepping stone for future BMEL work as additional testing modalities and more complicated orthopedic questions come into view. It is the hope that this work lays the foundation in developing new testing implements aimed towards preclinical applications.

1.1 Background & Motivation

The central challenge for an *in vitro* mechanical test is characterizing the relevant mechanical environment. In many cases, oversimplification or misidentification of a mechanical environment will lead to irrelevant data and wasted resources. For example, the supplementary experiments includes work on a biodegradable bone cuff device designed to repair comminuted fractures in long bones such as the femur. In previous studies of this device, the identified mechanical environment was uniaxial compression. Under such loading conditions, the cuff excelled; however, when implanted into an ovine model, the device immediately failed and the sheep was euthanized. The uniaxial compression test replicated a scenario where the device was longitudinally loaded by an animal statically standing. This scenario was irrelevant on two counts. First, device failure is highly unlikely to occur while the animal is standing still, but rather while the animal is running or standing up from a lying position. Second, unlike humans, the sheep femur is not longitudinal, but in a standing position is oriented at an approximately 45°angle with the ground. Thus, there is virtually no scenario in the ovine model wherein the cuff would be expected to experience uniaxial compressive loads. In addition to these analytic challenges, there are technical challenges in implementing relevant experiments. The scenarios discussed in orthopedic biomechanics are often complex and not often encompassed by the standard suite of experimental setups; in particular, the ubiquitous need for off-axis loading. [4, 5, 6, 7, 8, **?**] Traditional load frames exacerbate this problem in virtue of their uniaxial construction which affords only the flexibility to adjust the vertical location of the linear actuator and exchange instrumentation (in particular, load cells). Limited reconfiguration necessitates the researcher to manufacture custom fixturing and apparatuses for the system to perform the required mechanical scenario. [3] An alternative to traditional uniaxial systems are specialized simulation systems, such as the simVITRO robotic testing system. While such

systems can precisely simulate complicated physiological loading, they are often cost prohibitive and limited to a singular application. Additionally, biomechanical testing quite often involves the use of human cadaveric material which requires Biosafety Level 2 (BSL2) laboratory regulations. Acquiring BSL2 space for testing equipment often poses difficulties. The previous research in our lab sought to strike a middle path: devise a way to expand a load frame's physical functionality, and operate the system with a modular software to allow for easier expansion of the system at a lower cost. [3] To meet these technical needs, our lab developed a custom Reconfigurable Testing System (R.T.S.) to be permanently housed in a BSL2 space. By leveraging the modularity of LabVIEW software and 8020 extrusion hardware, this system is designed to reduce the initial cost, the time to design custom fixturing, and to allow for simpler expansion of the system on a project-to-project basis. [3]

Even with this newly developed equipment, the challenge arises in simplifying the scenarios such that they are experimentally manageable, yet remain mechanically relevant. The goal of this work is to develop and perform multi modal mechanical experiments with clinical and device applications in orthopedic biomechanics. The purpose of this suite of experiments is twofold. First and primarily, each experiment is individually designed to answer a specific subject matter question in the field of orthopedic biomechanics related to a novel surgical procedure or novel device. Experiment 1 evaluates a proposed novel method for repair of distal bicep tendon rupture, the double tension slide suturing technique; this is relevant as a potential new approach to repairing distal bicep tendon tears. Experiment 2 characterizes the strength of a novel shape memory polymer repair method for calvarial defect repair; this is relevant as the SMP is being developed for repair of craniomaxillofacial defects. Experiment 3 evaluates the cutting efficiency of different femoral broaching tools in canine total hip arthroplasty; this is relevant because of the high incidence of femoral fissure due to overbroaching sclerotic bone. Secondarily, taken together, these studies demonstrate the value of the reconfigurable testing system.

1.2 Specific Aims

Biomechanical experiments will be developed and performed using the R.T.S. Each experiment will be individually analyzed for its application in clinical orthopedic surgical practice or device development.

1.2.1 Specific Aim 1

Develop and perform clinically motivated biomechanical experiments with application in surgical orthopedics. **This specific aim will be considered met when at least one surgical technique has been tested and evaluated.**

1.2.1.1 Distal Bicep Tendon Repair

Design and perform experiment evaluating double tension slide suturing as a novel method for repair of distal bicep tendon rupture. This question is valid in its own right as a matter of innovative clinical practice. Fresh frozen human cadaveric elbows will have distal bicep tendon ruptures surgically induced and the matched pairs will be randomly separated into two cohorts for repair. The first cohort will undergo the clinically standard tension slide technique (TST) while the other cohort will undergo the novel double tension slide technique (DTS). Following these surgical procedures, the mechanical testing will proceed inspired by the methodology of Mazzocca et al. [9] Each elbow will be mounted anatomically to the R.T.S. using 8020 extrusions. Minimal soft tissue attachment will be removed in order to best preserve the normal physiological loading geometries. The proximal humerus will be fixed in place by two bolts and positioned to allow full extension at the elbow. A threaded intramedullary screw will be inserted into the distal radius. Once mounted, the tendon will be attached to the R.T.S. linear actuator using a stainless-steel serrated clamp with care taken to ensure each tendon is clamped above the sutures. A dead weight will be positioned to the threaded rod until a 50 N force is registered in the tendon, simulating the expected contracted force of the biceps in the early postoperative period based on previous post-surgical studies. The elbow joint will then be cycled from full extension to 90°flexion at a rate of 0.5 Hz for 3600 cycles in a preconditioning fatigue protocol. Following cyclic loading, the elbow will be fixed at

90°flexion and the tendon extended at a rate of 1 mm/sec until failure. Failure is defined as one of the following conditions: suture breakage, bone fracture, or tendon tear. Following failure, the soft tissue will be dissected to measure the diameter of the radius at the tuberosity. The difference in the load to failure between the groups will be analyzed using the paired t-test and the mode of failure will be compared between groups using the chi square test with significance set at $p < 0.05$. The bicep testing requires both difficult geometrical concerns (as it is a large joint) and fatiguing loading conditions. The testing modality in this subaim will be considered sinusoidal fatigue combined with uniaxial tension to failure.

1.2.2 Specific Aim 2

Develop and perform biomechanical experiments with device application in orthopedics. **This specific aim will be considered met when at least one device has been tested and evaluated.**

1.2.2.1 Shape Memory Polymer for Calvarial Defect Repair

Design and perform experiment characterizing the mechanical push-out properties of novel shape memory polymer for repair of craniomaxillofacial defects. This question is valid in its own right as a matter of technological innovation for physiological replication. Push-out tests are frequently used to evaluate the bone-implant interfacial strength of orthopedic implants, particularly dental and craniomaxillofacial applications. There currently is no standard method for performing push-out tests on calvarial models, leading to a variety of inconsistent approaches. In this study, fixtures and methods will be developed to perform push-out tests in accordance with the following design objectives: (i) the system rigidly fixes the explanted calvarial sample, (ii) it minimizes lateral bending, (iii) it positions the defect accurately, and (iv) it permits verification of the coaxial alignment of the defect with the push-out rod. The fixture and method will be first validated by completing push-out experiments on 30 explanted murine cranial caps and 2 explanted leporine cranial caps, all induced with bilateral sub-critical defects (5.5 mm and 8.0 mm nominal diameter for the murine and leporine models, respectively). Defects will be treated with an autograft (i.e., excised tissue flap), a shape memory polymer (SMP) scaffold, or a PEEK implant. Additional

validation will be performed on 24 murine cranial caps induced with a single, unilateral critically-sized defect (8.0 mm nominal diameter) and treated with an autograft or a SMP scaffold. This will provide important information about the mechanical integrity of the SMP treatment as well as provide a standardized approach to push-out testing in small animal calvarial studies. The testing modality in this subaim will be considered uniaxial push-out.

1.2.3 Specific Aim 3

Develop and perform biomechanical experiments with surgical instrument application in orthopedics. **This specific aim will be considered met when at least one instrument has been tested and evaluated.**

1.2.3.1 Femoral Broach for Canine Total Hip Arthroplasty

Design and perform experiment evaluating the cutting efficiency of different designs of femoral broaches for preparing canine femurs. This question is valid in its own right as a matter of technological innovation for surgical tools. Total hip replacement (THR) is a highly-successful treatment for pathologies of the canine hip such as hip dysplasia, femoral head or neck fracture, acetabular fracture, Legg-Calve-Perthes disease, or traumatic hip luxation. Cementless THR systems, the clinical standard, rely on a precision preparation and implantation technique in which the femoral implant and adjacent bone are in uniform contact along the entire implant surface. Initial implant stability is provided by friction between implant and bone, whereas long term stability occurs via bone ongrowth and ingrowth. Broaches are tooted devices that match the exterior geometry of the stem; they are driven into the reamed intermedullary cavity of the femur to prepare an envelope into which the stem is inserted by cutting and crushing the cancellous bone. Two complications are common: (1) fissure fracture in the femur due to hoop stresses are introduced to the bone from the broach (especially a risk for patients with high density, i.e. sclerotic, bone) and (2) post-operative subsidence of the femoral stem due to loss of press-fit. In this study, novel broach designs will be evaluated in terms of cutting efficiency and resistance to subsidence in polyurethane model bones (SawBones, Inc., WA, United States). Two densities will be considered: 15 pound per cubic foot

(pcf) to simulate the typical cancellous bone of a canine patient and 25 pcf to simulate the bone of a sclerotic patient.

1.3 Supplementary Experiments

In addition to the above, supplementary experiments are reported to further demonstrate the versatility of the Reconfigurable Testing Machine. Since they are not necessary for the specific aims to be met, but are nevertheless relevant to the present body of work, they are included in the appendix for reference.

1.3.1 Hip Capsulotomy Repair

Design and perform experiment evaluating the effect of capsulotomy repair in returning stability to the hip joint by way of strength of the hip suction seal. This question is valid in its own right as a matter of clinical practice. Fresh-frozen human cadavers from T12 vertebra to the distal end of the femurs will be dissected to remove unnecessary soft tissue, preserving only that architecture with non-negligible influence on hip joint mechanics. Each cadaver will be cut from the sacroiliac junction through the pubic symphysis to produce paired hip samples. Each hip sample will be attached to the R.T.S. in a carriage assembly designed for dual axis adjustment. Holes will be drilled into each anterior superior iliac spines (ASIS) for the placement of an angle guide to mark anatomically neutral position of each hip. Each hip sample will be serially adjusted into each of four configurations: physiological neutral, 10°abduction, 45°flexion, and "perpendicular", i.e., a simulation of the clinical joint stability evaluation wherein the loading line is perpendicular to the acetabular surface. The femur will be distracted at 1mm/s along the anatomical longitudial axis (for neutral, 10°abduction, and 45°flexion) or the clinically defined axis (perpindicular) until either reaching 400 N or 15 mm, conditions deemed to be damaging to the tissue. Maximum extension will be kept constant for each sample. Following baseline evaluation (i.e. all soft tissue intact), the mechanical testing regimen will be serially repeated for each hip following Inter-Portal Capsulotomy, T Capsulotomy, Partial Repair (or single repair), and Full Repair (or double repair). Maximum load achieved prior to failure of the suction seal will be the data point of interest.

ANOVA with Tukey post-hoc will be used to calculate statistical significance. The large hip joint poses significant geometrical challenges that could not be met by way of a traditional machine.

1.3.2 Biodegradable Fracture Fixation Cuff

Design and perform experiment evaluating the mechanical behavior of a biodegradable cuff for repair of comminuted long bone fracture. This question is valid in its own right as a matter of technological innovation for fracture repair. Surgical autografting of bone defects has significant limitations; there is a pressing need for a biodegradable implant that promotes bone regeneration in critical size defects while also providing the mechanical stability required during the healing period. A load bearing fracture fixation device consisting of a biodegradable polymer tube, manufactured from poly-(ester urea) (PEU) has been designed to support critical size defects in long bones during recovery after a comminuted fracture and ultimately lead to healing. While it is important that the device be biodegradable to preclude the need for secondary surgery once the defect has been healed, it is crucial that the degradation experienced by the device inside the body does not compromise its mechanical strength before bone strength is sufficiently restored. It is therefore desirable to subject the device to degradation *in vitro* to study the effects on its mechanical performance. These devices will be subjected to short term degradation and the effects on failure strength and fracture development will be investigated. Fixation devices will be installed into the R.T.S. and tested under a 4-point bending configuration to simulate a worst-case-scenario mechanical load for an ovine animal model. PEU shells will be tested under two conditions: dry or 1 hour degradation. For the dry condition, sterile, injection molded devices will be removed from their packaging, photographed, and subjected to ramp to failure in 4-point bend configuration. The 4 point bend setup will have a 4 inch lever arm and the ramp will run at approximately 24°/second until failure. For the 1 hour degradation condition, devices will be submerged in a saline bath at 37°Celsius and simultaneously subjected to a static bending torque of 200 in-lbf. After the hour has passed, the degraded device will undergo the 4-point bend ramp to failure protocol. Following the ramp to failure, each shell will be reconstructed and photographed to qualitatively characterize the fracture patterns. Welchs t-tests will be used to analyze statistical differences in failure torques

(calculated as failure load multiplied by the length of the lever arm) between each of the fracture pattern types, as well as between the degraded and dry groups. The characterization testing requires a 4 point bend with a fairly large footprint.

1.4 Other Study Information

1.4.1 Texas A&M Institutional Biosafety Committee

Human cadaveric work conducted under IBC permit **IBC2017-037 Moreno - Biomechanical Environments Laboratory -** ***Biomechanical Testing of Cells and Tissues***. Approved: June 19, 2017 / Expires: June 19, 2020.

1.4.2 Texas A&M IACUC

Animal cadaveric work conducted under AUP 2016-0348.

2. BIOMECHANICAL EVALUATION OF DOUBLE TENSION SLIDE TECHNIQUE AS A NOVEL REPAIR OF DISTAL BICEPS TENDON RUPTURE

This section is derivative of Sochacki, K. R., Jack, R. A., Lawson, Z. T., Dong, D., Robbins, A. B., Moreno, M. R., & McCulloch, P. C. (2020). Distal Biceps Tendon Repair Using a Double Tension Slide Technique. Arthroscopy Techniques. and Sochacki, K. R., Lawson, Z.T., Jack, R. A., Dong, D., Robbins, A. B., Moreno, M. R., & McCulloch, P. (2021). Double Tension Slide Technique as a Novel Repair for Distal Biceps Tendon Tear: A Biomechanical Evaluation. Cureus, 13(3). Used with permission: "As the author of this Elsevier article, you retain the right to include it in a thesis or dissertation, provided it is not published commercially. Permission is not required, but please ensure that you reference the journal as the original source."

2.1 INTRODUCTION

Rupture of the distal biceps brachii tendon usually occurs in the dominant arm of men between 40 and 60 years of age, inhibiting the biceps primary functions of elbow flexion, extension, pronation, and supination. This injury is thought to occur as a result of an acute forceful eccentric load on a degenerative tendon. [10, 11] Non-operative treatment following rupture leads to significantly decreased forearm supination and elbow flexion strength. [11, 12, 13, 14] Thus, primary operative repair is recommended for active patients as it can restore function to near normal levels. [11, 15, 16, 17, 18, 19] Several different methods of distal biceps tendon reattachment have evolved over the years including the bone tunnel technique, suture anchor repair, interference screw, and cortical button. [10, 15, 12, 20, 21, 22, 13, 23, 24, 25, 26, 27] One technique that has shown mechanical stability and allowance of early range of motion in patients is the cortical button fixation technique, described by Bain et al, which uses Smith & Nephews EndoButton fixation device to reattach the biceps to an anterior insertion in the radius. Biomechanical studies have compared the different repair methods with suspensory cortical button frequently having the highest load to failure. [28, 17, 21, 22, 23, 25] The tension slide suturing technique (TST) with inference screw

was then developed by Sethi et al. demonstrating greater load to failure and less gap formation compared to traditional fixation with cortical button. [29, 30] Proven stability throughout multiple biomechanical studies has allowed the cortical button technique to be used as a reference point to evaluate the efficiency of novel approaches. [30] In particular, there have been reports of interference screw failure following its use in distal biceps repair with an increased risk of fracture through the bone tunnel. [18, 19] This has led to several surgeons to abandon interference screws in favor of a single suture TST fixation with a cortical button. In this approach, a single needle is woven down the middle of the distal tendon such that a single suture thread is attached to the cortical button and the two strands of the single suture are tied to each other. As such, rupture of either strand or loss of knot security would yield complete loss of initial fixation. Concerns over the biomechanical strength of the TST suturing technique led to the development of the double tension slide technique (DTS) which employs two self-tightening sutures (one on each side of the tendon) such that two suture threads attach to the cortical button. [31] Previous biomechanical studies involving distal biceps tendon repairs have not adequately evaluated this technique. The purpose of this study was to perform a comparative biomechanical investigation of two alternative approaches for distal biceps tendon repair: a single suture tension slide technique (TST) and two suture double tension slide (DTS) technique, with the hypothesis of no difference between the two techniques.

2.2 METHODS

Ten matched pairs of fresh frozen human cadaveric elbows (20 elbows, mid forearm to mid humerus) were randomly assigned to one of two cohorts. In the first cohort, the bicep tendon was repaired using the tension slide technique (TST) as described by Sethi et al. [29, 30] The other cohort was repaired using the novel double tension slide technique (DTS). A longitudinal incision was made along the medial border of brachioradialis and dissection carried down to the distal biceps tendon insertion on the radial tuberosity. The distal biceps tendon was then sharply removed from the radial tuberosity.

2.2.1 Surgical Technique

The tension side technique (TST) was performed using the technique described by Sethi et al. [29] without the use of an interference screw. A single No. 2 high tension non-absorbable composite suture (FiberLoop, Arthrex, Naples, FL) with straight needle was used to secure the distal 2.5 cm of the biceps tendon in a locking-loop fashion. Each limb of the suture was then passed through the biceps button (Arthrex, Naples, FL) as described. The double tension slide technique was performed with two No. 2 high tension non-absorbable composite suture (FiberWire, Arthrex, Naples, FL). Our surgical collaborators at Houston Methodist prefer to use a blue suture and tiger suture for ease of suture management. The first suture was passed through the distal biceps tendon starting at the medial and distal aspect of the tendon running proximally 2.5 cm in a locking fashion and then back distally exiting 1 cm from the distal tendon. This was then repeated with the second suture starting at the lateral and distal aspect of the tendon. The two central strands of the sutures were then threaded through the cortical button (BicepsButton, Arthrex, Naples, FL) in opposite directions. The central strand of the medial (tiger) suture was inserted through the medial hole and then back through the lateral hole. The central strand of the latera (blue) suture was then inserted through the lateral hole and then back through the medial hole. Both strands that were passed through the biceps button were then facing toward the distal biceps tendon. In both cohorts, a 3.2-millimeter (mm) (Arthrex, Naples, FL) guide pin was drilled through then center of the radial tuberosity from anterior to posterior. The anterior cortex was then reamed with an 8.0-mm cannulated reamer (Arthrex, Naples, FL). The guide pin was removed and a button inserted was used to pass the biceps button through the 3.2-mm hole in the tuberosity from anterior to posterior. The button was then released from the holder and the biceps button was flipped. The two limbs of suture passed through the button were then toggled to dock the biceps tendon into the bone socket. Once the biceps tendon was fully seated in the socket, the two limbs of the same suture were tied together for both the medial (tiger) and lateral (blue) sutures. Finally, the sutures that passed through the button (one tiger and one blue) were tied together to reinforce the construct.

The patient is placed in the supine position on a hand table. The injured arm is then prepared

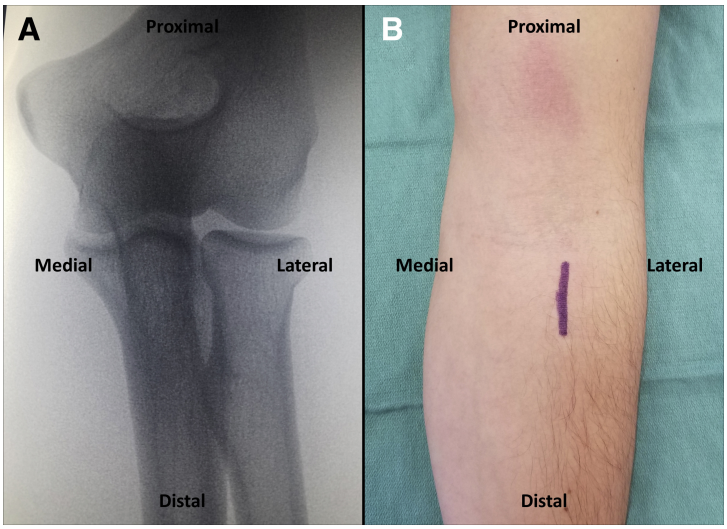

Figure 2.1: (A) Intraoperative fluoroscopy of right elbow demonstrating location of radial tuberosity localization prior to incision. (B) Intraoperative image of right arm with planned 3-cm incision along medial border of brachioradialis centered over the radial tuberosity.

Figure 2.2: Right elbow. The first suture is passed through the distal biceps tendon starting at the medial and distal aspect of the tendon running proximally 2.5 cm in a locking fashion and then back distally exiting 1 cm from the distal tendon.

and draped using the surgeon's preferred method similar to other distal bicep tendon repairs, and a sterile tourniquet is placed on the upper arm. Fluoroscopy is used to identify the site of the radial tuberosity. An approximate 3-cm incision is then made along the medial border of the brachioradialis centered over radial tuberosity distal to the flexion crease (Fig. 2.1). Blunt dissection is carried

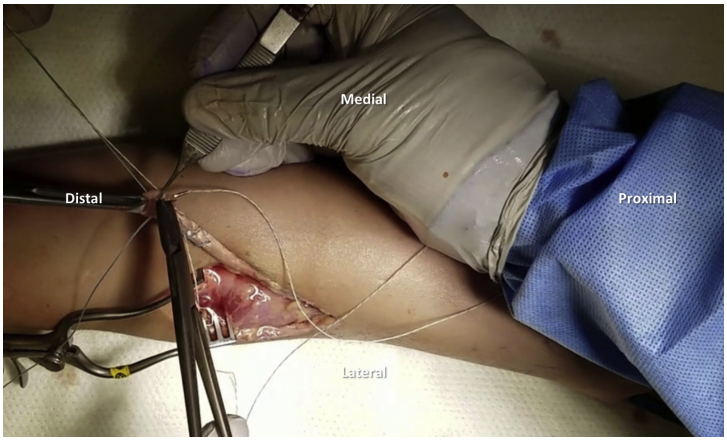

Figure 2.3: Right elbow. The second suture is passed through the distal biceps tendon starting at the lateral and distal aspect of the tendon.

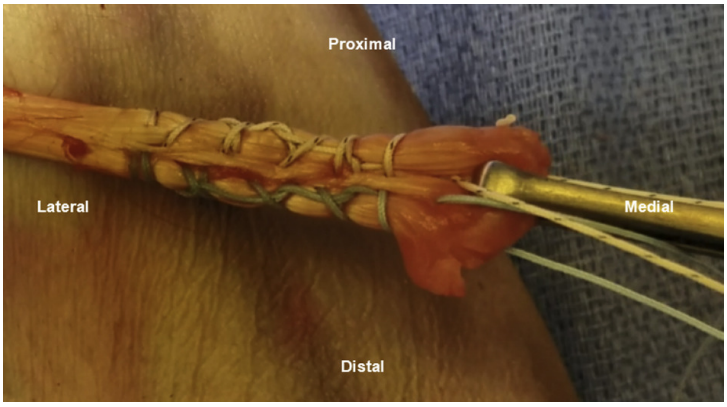

Figure 2.4: Right elbow with biceps tendon stumped pulled proximal out of the wound. This demonstrates the finished product after both sutures have been passed through the distal biceps tendon. Both sutures exit 1 cm from the distal tendon

down to the radial tuberosity and proximally to identify the tendon stump. During dissection, the lateral antebrachial cutaneous nerve is identified and protected. Adhesions are released from the tendon, and the tendon stump is then debrided to normal healthy appearing tendon. The double tension slide technique is performed with 2 No. 2 high tension nonabsorbable composite suture (FiberWire, Arthrex, Naples, FL). Our surgical collaborators at Houston Methodist prefer to use a blue suture and tiger suture for ease of suture management. The first suture is passed through the distal biceps tendon starting at the medial and distal aspect of the tendon running proximally

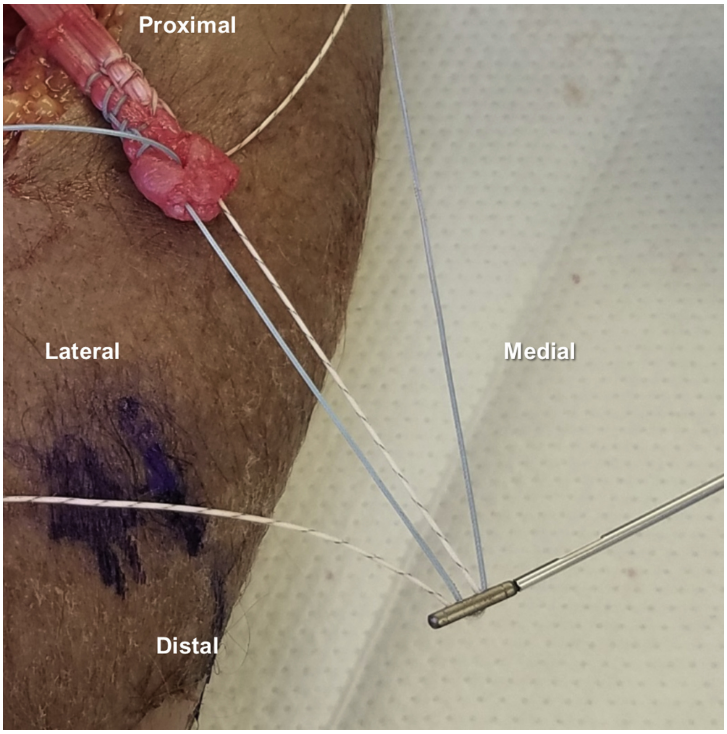

Figure 2.5: Right elbow. The 2 central strands of the sutures are threaded through the cortical button in opposite directions. The central strand of the medial (tiger) suture is inserted through the medial hole and then back through the lateral hole. The central strand of the lateral (blue) suture is then inserted through the lateral hole and then back through the medial hole. Both strands that are passed through the biceps button are then facing toward the distal biceps tendon.

2.5 cm in a locking fashion and then back distally exiting 1 cm from the distal tendon (Fig 2.2). This is then then repeated with the second suture starting at the lateral and distal aspect of the tendon (Fig 2.3). The 2 central strands of the sutures are then threaded through the cortical button (BicepsButton, Arthrex) in opposite directions. The central strand of the medial (tiger) suture is inserted through the medial hole and then back through the lateral hole. The central strand of the lateral (blue) suture is then inserted through the lateral hole and then back through the medial hole (Fig 2.4). Both strands that are passed through the biceps button are then facing toward the distal biceps tendon (Fig 2.5). With the arm in maximal supination a 3.2-mm (Arthrex) guide pin is drilled through the center of the radial tuberosity from anterior to posterior taking care to avoid the posterior interosseous nerve. This is done using fluoroscopy (Fig 2.6). The anterior cortex is then reamed with an 8.0-mm cannulated reamer (Arthrex) (Figs 2.7 and 2.8). The guide pin is

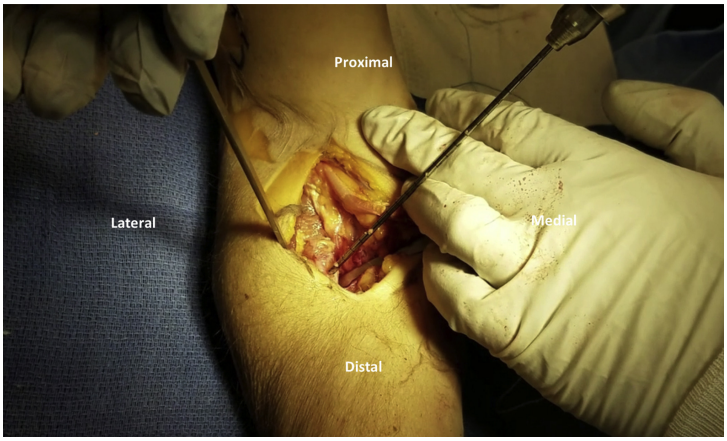

Figure 2.6: With the right arm in maximal supination a 3.2-mm guide pin is drilled through the center of the radial tuberosity from anterior to posterior taking care to avoid the posterior interosseous nerve (PIN). This is done using fluoroscopy.

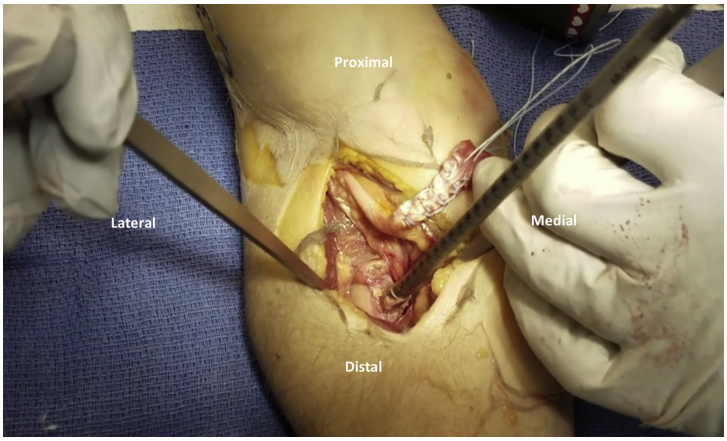

Figure 2.7: Right elbow. The anterior cortex is then reamed with an appropriately sized cannulated reamer.

removed and the button inserter was used to pass the biceps button through the 3.2-mm hole in the tuberosity from anterior to posterior (Fig 2.9). The button is then released from the holder and the biceps button is flipped against the posterior cortex of the radius. The 2 limbs of suture passed through the button are then toggled to dock the biceps tendon into the bone socket (Figs 2.10 and 2.11). Once the biceps tendon is fully seated in the socket, the 2 limbs of the same suture are tied together for both the medial (tiger) and lateral (blue) sutures. Finally, the sutures that passed

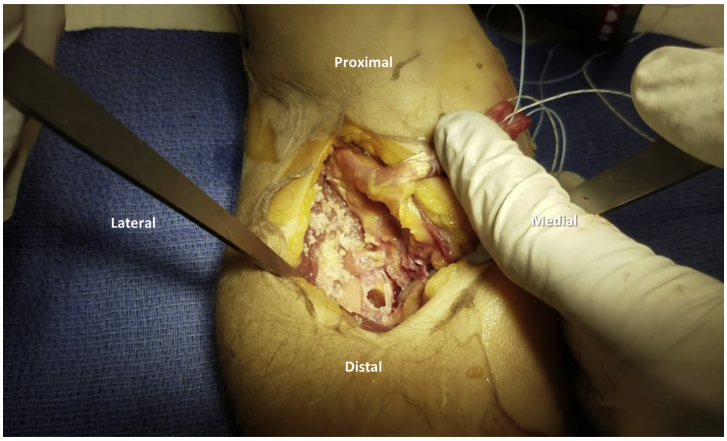

Figure 2.8: Right elbow. The guide pin is then removed leaving a unicortical bone socket for the tendon to be docked into.

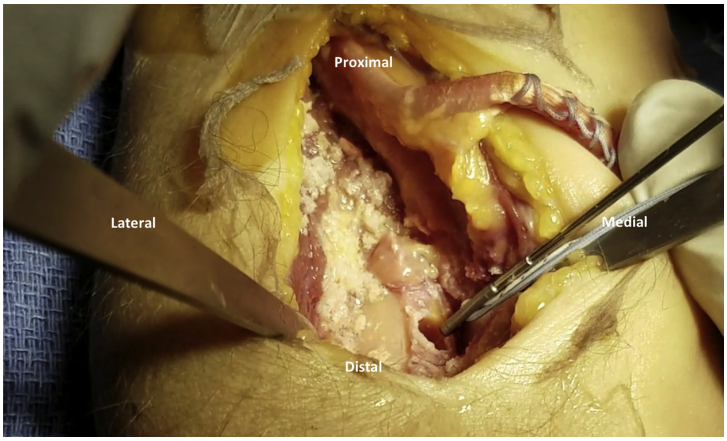

Figure 2.9: Right elbow. After reaming the appropriate-sized tunnel in the radial tuberosity, the button inserter is used to pass the biceps button through the 3.2-mm hole in the tuberosity from anterior to posterior. The button is then released from the holder and the biceps button is flipped against the posterior cortex of the radius.

through the button (1 tiger and 1 blue) are tied together to reinforce the construct (Figs 2.12 and 2.13). Final anteroposterior and lateral fluoroscopy views are used to demonstrate that the button is in an appropriate position and the tendon is reduced into the socket (Fig 2.14). The wound is then irrigated and closed in a layered fashion with absorbable suture followed by a posterior long arm splint with the arm in neutral rotation and flexed to its resting tension following the repair. The splint is kept in place for one week followed by placement of a hinged elbow brace for 6 weeks.

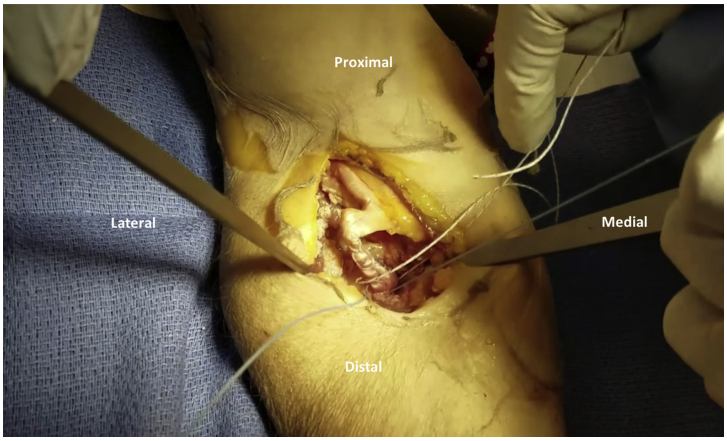

Figure 2.10: Right elbow. The 2 limbs of suture passed through the button are then toggled to dock the biceps tendon into the bone socket.

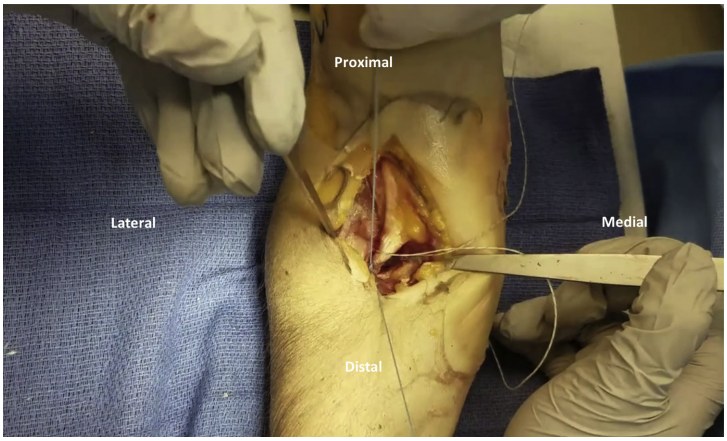

Figure 2.11: Right elbow. The tendon is then confirmed to be completely docked into the tunnel after tensioning the sutures.

The brace is set so that the patient can obtain full flexion but extension is limited to the resting tension of the repair. Extension is advanced 20ř per week until full extension is achieved. The elbow brace is then removed after 6 weeks and the patient is allowed to use the arm for all activities of daily living with limited weight bearing until 3 months postoperatively. At that time, the patient can start progressive biceps strengthening exercises.

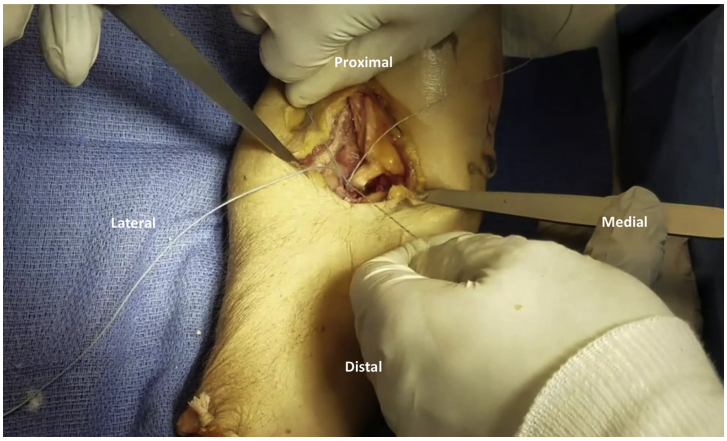

Figure 2.12: Right elbow. Once the biceps tendon is fully seated in the socket, the 2 limbs of the same suture are tied together for both the medial (tiger) and lateral (blue) sutures. Finally, the sutures that passed through the button (1 tiger and 1 blue) are tied together to reinforce the construct.

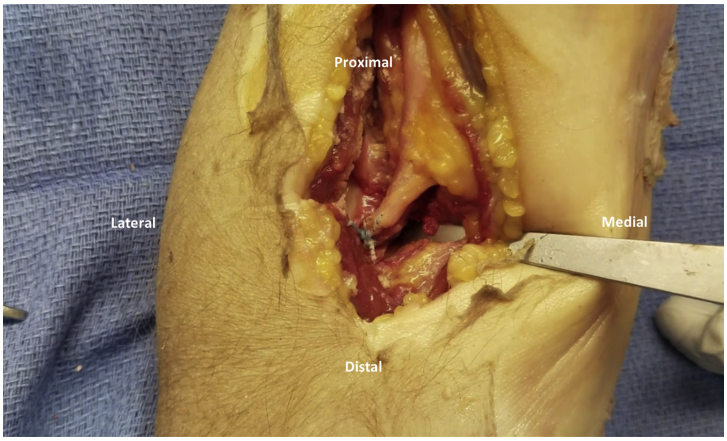

Figure 2.13: Right elbow. The limbs of the sutures are then cut leaving a short tail.

2.2.2 Mechanical Testing

Each specimen was then mounted to Reconfigurable Testing System (R.T.S.) in the systems linear configuration. An effort was made to preserve as much of the soft tissue attachments as possible in order to preserve the normal physiological loading geometries. The humerus was fixed vertically with bolts and positioned to allow for full extension of the elbow. A threaded intramedullary screw was inserted into the distal radius to allow for fixation of dead weight representing the hand

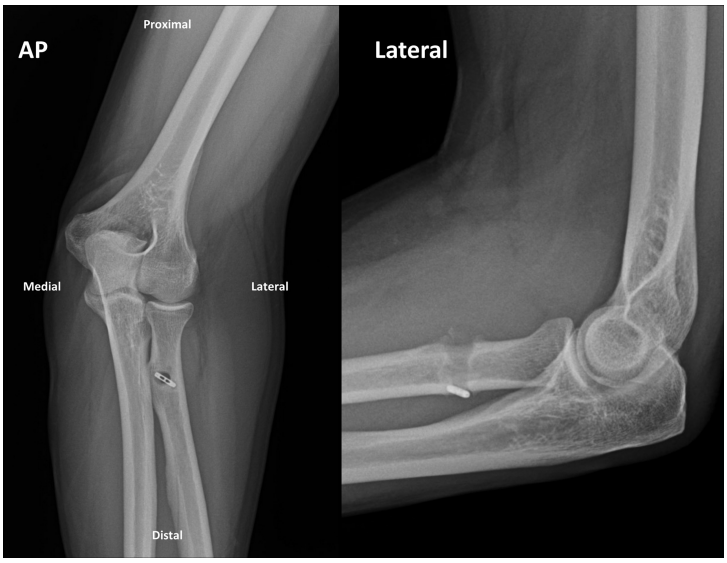

Figure 2.14: Final anteroposterior and lateral fluoroscopy views of the right elbow are used to demonstrate that the button is in an appropriate position and the tendon is reduced into the socket.

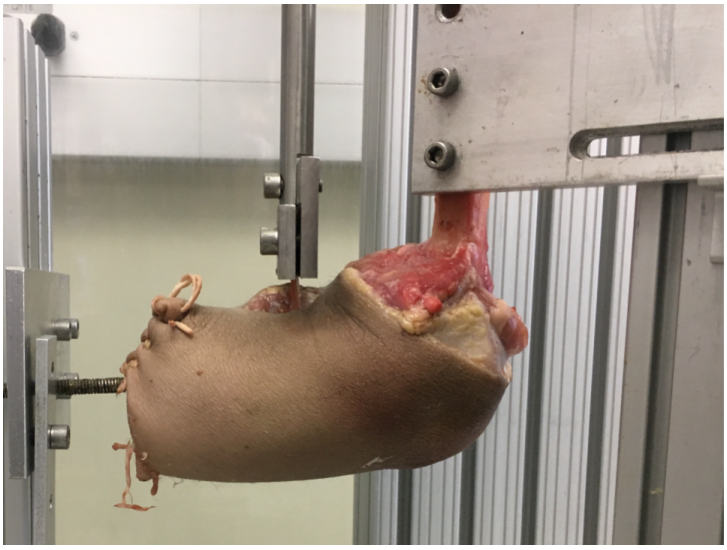

Figure 2.15: Specimen locked at 90°flexion for ramp testing.

and for rigid fixation. After securing the humerus in place, a stainless steel dead weight corresponding to 50 N force was attached to the intramedullary rod in the radius. This pre-load was based on the expected passive contraction force of the biceps tendon in the early postoperative period based on previous postsurgical studies. [16] The tendon was clamped above the sutures to

the R.T.S. crosshead using custom, sinusoidal stainless steel clamps. [32] With the 50 N pre-load in place, the elbow was brought to 90°flexion; calipers were used to measure the distance between the bottom of the clamps and the top of the radial tuberosity and recorded as the pre-fatigue tendon gage length. The elbow joint was then cycled from full, natural extension to 90°flexion at a rate of 0.5 Hz for 3600 cycles in a preconditioning fatigue protocol. After fatigue testing, the joint was brought back the 90°flexion to record the post-fatigue tendon gage length; gapping was defined as the difference between the pre- and post-fatigue gage lengths. The 50 N dead weight was then removed to lock the intramedullary rod in place. With the specimen locked at 90°flexion, the tendon was ramped at 1mm/sec until the repair construct failed (Fig 2.15). Failure conditions were defined as (i) suture breakage, (ii) bone fracture, or (iii) tendon pulled free from suture. [22] Specimens that sustained radial fracture at the interface of the threaded intramedullary screw prior to failure were excluded from analysis. The failure mode for each sample was recorded. Following failure, the soft tissue was dissected to measure the diameter of the radius at the tuberosity. Load-displacement charts were generated for each specimen; a linear region was identified and linear regression taken to calculate a stiffness value (N/mm) for the tendon-suture-button construct. The difference in failure load, construct stiffness, and gapping between TST vs DTS cohorts was analyzed using paired Welchs t-test. The mode of failure was compared between groups using the chi square test. All p values were reported with significance set at $p < 0.05$.

2.3 RESULTS

One matched specimen sustained radial shaft fracture at the bone-screw interface of the intramedullary screw prior to construct failure; both specimens of this matched pair were excluded from analysis. Nine matched (n=18) pairs were included in final analysis. All specimens were male (mean age of 48.9 $\pm$ 14.3 years old, height 71.2 $\pm$ 2.6 inches, weight 173.5 $\pm$ 44.4 pounds, and radius diameter 17.2 $\pm$ 0.9 millimeters).

None of the included specimens failed during preconditioning with cyclic loading. The mean failure load in the DTS group was 383. 3 $\pm$ 149.3 Newtons (N) compared to 275.8 $\pm$ 98.1 N in the TST group (p=0.12, paired t-test) (Fig 2.16). The mean stiffness for the DTS group was

29.94 $\pm$ 9.71 N/mm compared to 32.47 $\pm$ 11.51 N/mm for the TST group (p = 0.13). The average change in tendon gage length was 9.54 $\pm$ 4.98 mm for the DTS group compared to 7.04 $\pm$ 9.31 mm for the TST group (p=0.55). The gapping variance for the TST group was 86.6. The mode of failure for the DTS specimens occurred at the tendon (n=5), suture (n=3), and bone (n=1). The specimens fixed with the TST technique failed at the tendon (n=4) and suture (n=5) only. There was no significant difference in failure type between groups (p=0.76).

The mode of failure for the DTS specimens occurred at the tendon (n=5), suture (n=3), and bone (n=1). The specimens fixed with the TST technique failed at the tendon (n=4) and suture (n=5) only. There was no significant difference in failure type between groups (p=0.76). In summary, the two suture methods did not perform significantly different under any of the testing criteria.

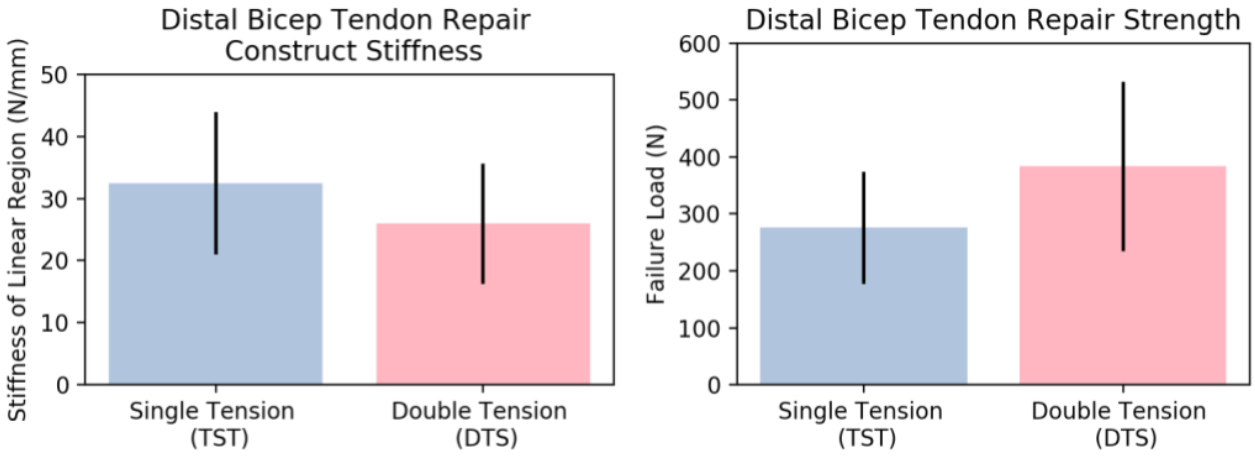

Figure 2.16: Left: Stiffness of the constructs, Right: Load at failure of the constructs

2.4 DISCUSSION

It was determined that the double tension slide technique and the tension slide technique had similar biomechanical strengths with a non-significant trend favoring the DTS technique having a superior load to failure.

Several single and two incision techniques for distal biceps tendon repairs have been described with bone tunnels, suture anchors, interference screws, and cortical buttons. [10, 21, 22, 13, 23, 25, 26] Sethi et al. demonstrated that the single incision tension slide technique with interference screw had the strongest biomechanical properties. [29, 30] However, reports of interference screw failure with increased risk of fracture through the bone tunnel led to the described development of the double tension slide technique (DTS).[22, 18, 19, 33]

Intuitively, one would think adding a second suture would increase the strength of the repair, but this had not been previously investigated. Furthermore, the redundancy of a second suture should provide a failsafe if either strand of the initial sutures was damaged by the needle, abrasion against the bone, or loss of knot security at the button.

The mean load to failure was similar between the DTS and TST groups (383. 3 ± 149.3 N vs 275.8 ± 98.1 N, respectively). Although not statistically significant, there was a trend in favor of the DTS technique with 7 of the 9 matched pairs having superior strength compared to the TST. The failure loads are comparable to previous studies which report values ranging from 259 N to 440 N using suspensory cortical button fixation with the TST fixation. [17, 22, 27, 29, 30] Due to the inherent differences of each biomechanical study (cadaver quality, testing machine, soft tissue envelope), it is difficult to perform inter-study comparisons.

The mechanism of repair failure did not differ between groups with similar numbers of suture breakage and tendon failure. This differs from the study by Sethi et al. in which the construct was more likely to fail at the tendon-suture interface compared to suture rupture. [30] Interestingly, both studies used the same suture.

There are limitations to this study. This study was limited by the small number of specimens and its associated low power. A post-hoc power analysis demonstrated that 26 matched pairs would be needed for 80% power at = 0.05 under a two-tailed t-test. This limitation is not unique to the current study, and it is commonly associated with biomechanical testing where obtaining an adequately powered sample size would be cost prohibitive. Bone mineral density (BMD) of the specimens was not analyzed; however, due to the use of matched pairs, there is likely to be little

variation in BMD. We attempted to maintain as many soft tissue attachments as possible during the repair technique and biomechanical testing in order to best preserve the normal physiological loading geometries. However, as with many biomechanical studies, the present study was unable to completely replicate the complex loading forces on the repaired tendon as seen in vivo with the combination of flexion, extension, pronation, and supination. It is unclear what load to failure value is clinically relevant in the early postoperative period to prevent repair failure. As such, the stronger repair demonstrated by the DTS technique might not be clinically necessary assuming that the single suture and knot security are not compromised and should be investigated in future studies.

2.5 CONCLUSION

In conclusion, the double tension slide technique demonstrates a greater, but similar load to failure as the tension slide technique; the redundancy provided by the second suture has an inherent advantage without compromising the biomechanical performance. The DTS technique maintains the many potential advantages to the tension slide technique without the risk of bone tunnel fracture with an interference screw. Intuitively, the addition of a second suture would likely increase the strength of the repair, but this had not been previously investigated. Furthermore, the redundancy of a second suture should provide a failsafe if either strand of the initial sutures was damaged by the needle, abrasion against the bone, or loss of knot security at the button. By passing 2 sutures through the tendon, the present technique increases the cross-sectional area of tendon in contact with suture to reduce the force transmitted through the individual passes of the suture and reduce failure at the tendon-suture interface.

3. BIOMECHANICAL PUSH-OUT EVALUATION OF BIOACTIVE, SELF-FITTING SHAPE MEMORY POLYMER SCAFFOLDS TO TREAT CRANIAL BONE DEFECTS

This section draws from Lawson, Z. T., Han, J., Saunders, W. B., Grunlan, M. A., Moreno, M. R., & Robbins, A. B. (2021). Methodology for Performing Biomechanical Push-Out Tests for Evaluating the Osseointegration of Calvarial Defect Repair in Small Animal Models. MethodsX, 101541. and its co-submission Pfau, M.R., Beltran, F.O., Woodard, L.N., Dobson, L.K., Gasson, S.B., Robbins, A., Lawson, Z.T., Saunders, W.B., Moreno, M.R., & Grunlan, M. A. (2021). Evaluation of a Self-Fitting, Shape Memory Polymer Scaffold in a Rabbit Calvarial Defect Model. Acta Biomaterialia. Used with permission: "As the author of this Elsevier article, you retain the right to include it in a thesis or dissertation, provided it is not published commercially. Permission is not required, but please ensure that you reference the journal as the original source."

3.1 INTRODUCTION

Confined craniomaxillofacial (CMF) defects may be caused by a tumor, infection (osteomyelitis), trauma, or surgical burr holes from craniotomies. The leading treatment option is autologous bone grafts; however, the autograph approach is limited by difficulty harvesting and shaping the autograft to tightly fix into the defect. Tissue engineering approaches have produced promising alternatives in terms of matching defect geometry and promoting bone healing. To this end, a moldable shape memory polymer (SMP) scaffold has been developed with tunable degradation, pore interconnectivity, bioactivity, and self-fitting into irregular model defects[34]). To be a successful device, the SMP implant must show favorable mechanical performance in comparison to the autograft standard. The push-out test is a common method for assessing the mechanical strength of the bone-implant interface in craniomaxillofacial applications. In particular, the cranial defect model poses unique challenges in experimental design. Cranial caps, especially for small animal models, possess significant curvatures which complicate the process of clamping without inducing significant stresses into the specimen. Figure 3.1 illustrates the generic push-out test set-up with

important geometrical parameters.

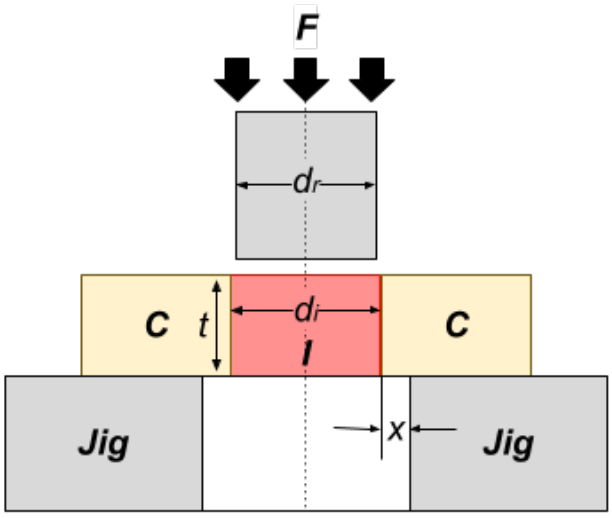

Figure 3.1: Schematic drawing of a generic pushout test, adapted from Dhert et al. [1] F = force applied on implant; I = implant; C = cortex of bone; Jig = support jig; x = clearance of hole in support jig, di = implant diameter, dr = push-out rod diameter = cortical thickness.

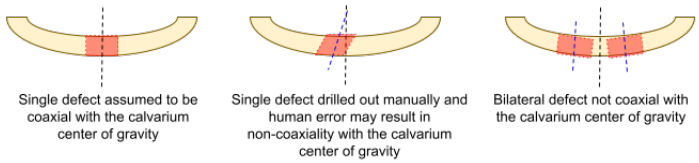

Figure 3.2: Illustration of the geometrical difficulties associated with current single and bilateral defect models.

In a seminal 1989 article. [35], Jonathan Black listed several factors which should be reported when performing calvarial push-out tests, including: (a) specimen geometry, (b) defect alignment, (c) mounting method, (d) fit of support jig, (e) load-displacement protocol, and (f) push-out rod and clearance hole geometry. While many researchers report the geometry and loading protocol, the alignment and fixation methods were found to be rarely reported in the literature.

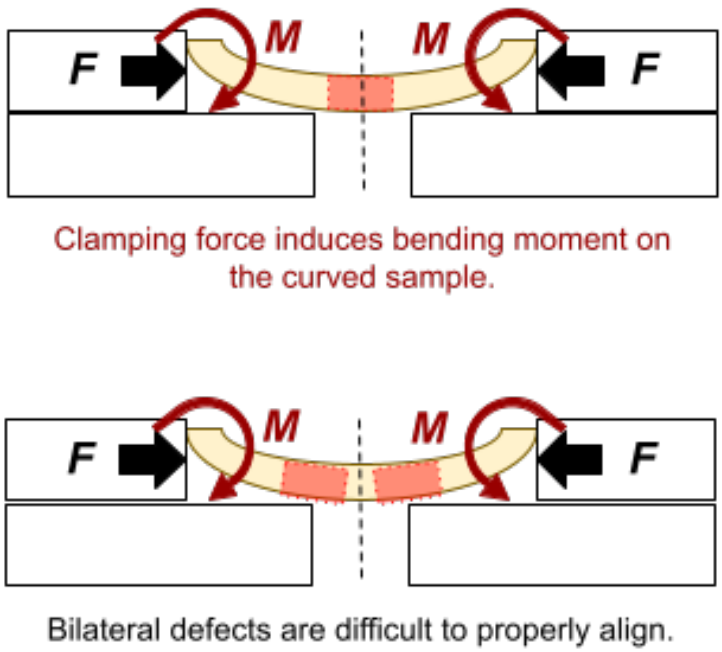

Figure 3.3: Schematic of a current lateral clamping method with single defect model (top) and bilateral defect model (bottom). Where F = lateral clamping force and M = moment induced due to the curvature of the specimen.

Initially, a simple method was attempted, loosely based on reports in the literature. [36, 37] by clamping the two distal ends of a rectangular specimen. However, such a method does not, on its own, ensure coaxial alignment with the push-out rod's line of action. For single critical defect models, coaxial alignment is assumed in virtue of the geometry of the skull; while this assumption is questionable in its own right, it is clearly not accurate in bilateral defect models (Figure 3.2). Additionally, lateral compressive clamping on the distal ends interacts with the samples' curvature and imposes a significant bending moment on the sample (Figure 3.3). To address these issues, four design criteria were established to support an improved calvarial defect pushout testing apparatus. The apparatus should

1. rigidly fix the explanted calvarial sample,

2. minimize lateral bending and the resulting internal stresses,

3. position the defect accurately, and

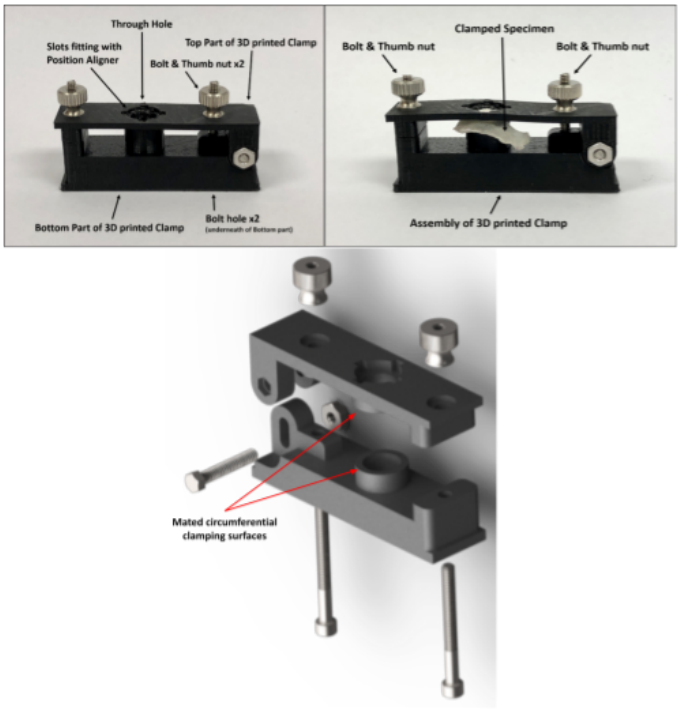

Figure 3.4: Fully assembled clamp (top left) and with specimen (top right). Exploded view (bottom).

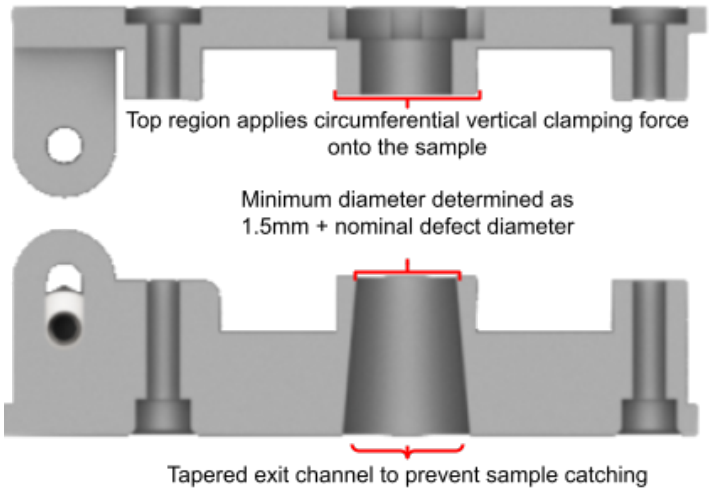

Figure 3.5: Sectional of the exploded view.

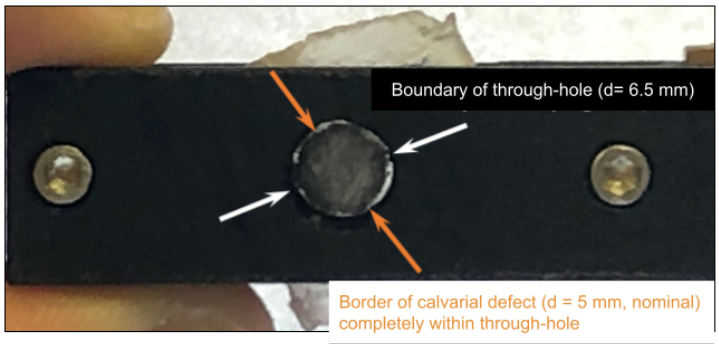

Figure 3.6: The boundary of the defect is verified to be within the boundary of the through-hole by shining a light through the hole. Note: pictured is the murine calvarial defect, hence the 5 mm nominal diameter.

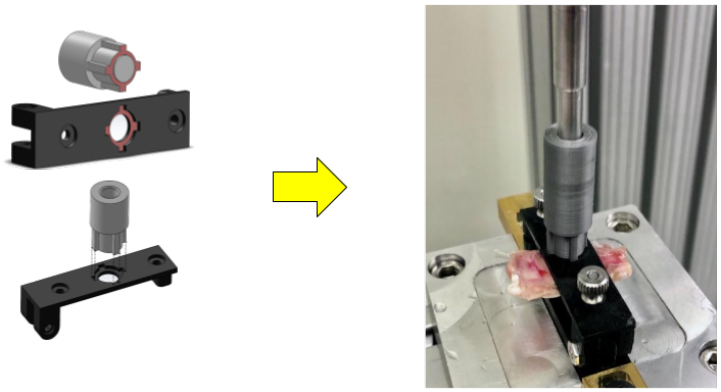

Figure 3.7: Illustration of the targeted notch mating geometry (left). Verification of the push-out rod's alignment with the clamping fixture with murine bilateral defect calvarial sample (right).

4. permit verification of the coaxial alignment of the defect with the push-out rod.

A new test method and apparatus was developed for performing push-out tests on cranial defects in small animal models that meets these requirements and can be used to evaluate novel calvarial defect therapies in comparison to gold standard therapies. These were used to evaluate the novel SMP device in comparison with the gold standard.

3.2 METHODS

3.2.1 Fixture Design

3.2.1.1 1. Clamping Without Deforming Under Load

The core component of our fixtures is a custom 3D printed hinged clamp with a through-hole which circumferentially clamps onto the calvarial sample (Figure 3.4 The circumferential clamping permits fixation of the specimen while minimizing the bending that is induced in the skull as a result of skull curvature; the circumferential clamping surface is relatively narrow to introduce minimal bending. In practice, these clamps were 3D printed on a MakerBot Replicator 2X 3D printer. Acrylonitrile butadiene styrene (ABS) plastic was printed at 80% infill. Although poly(lactic acid) (PLA) filament may also work, it is better practice to use ABS when printed parts are used in a mechanical application, especially if exposed to moisture as is the case here. The fixture applies a vertical clamping force by thumb tightened nuts. Since during the pushout test the sample is loaded in downward compression, it was found that only a moderate compression of the clamp was required to achieve specimen fixation during handling. The diameter of the through hole in the clamp (i.e., the hole through which the implant is pushed-out) was determined according to the rule laid out by Dhert, et al. [1], that the minimum clearance between the defect and the through-hole should be 0.7 mm (i.e., add 0.7 mm to the radius of the defect) (Figure 3.5). Additionally, to account for the 100 m tolerance of the 3D printer, an additional 0.05 mm was added to the nominal radius of the defect in each case; for a mouse model defect with a nominal diameter 5 mm the hole had a diameter of 6.5 mm, and for the rabbit model with a nominal defect diameter of 8 mm the hole diameter was 9.5 mm. For added clearance, the through-hole was printed with a slight downward and outward taper (i.e., the opening at the bottom was larger than the opening in contact with the calvarium) to reduce the opportunity of the dislodged tissue catching on the interior sides of the device.

3.2.1.2 2. Specimen-Fixture Alignment

Alignment of the specimen in the fixture is critical; poor alignment results in the implanted device catching the sides of the through hole as it is pushed out, resulting in measured loads that are unrelated to the disengagement of the device from the bone. In this design, defect alignment may be verified by shining a light through the bottom of the clamp and visually confirming the entirety of the defect is within the perimeter of the through hole (Figure 3.6). While this may not work for all combinations of implant materials and animal models, in cases reported herein, the alignment was easily verified.

3.2.1.3 3. Fixture-Machine Alignment

Lastly, the design must enable easy alignment of the clamping fixture to the testing machine axis. In particular, since the specimen is typically clamped while the 3D printed fixture is detached from the machine, alignment must be performed with each use of the clamp and must be fast and accurate. To this end, the top surface of the clamping fixture includes a targeted notch pattern centered on the through-hole (Figure 3.7). A removable mating alignment cylinder was 3D printed with the inverse of the targeted notch pattern, which can be attached to the pushout rod. In order to align the clamping fixture with the machine axis, while the specimen is clamped in place, the clamping fixture can be secured with its base which is attached to a Newport M-461 linear stage. The push out rod can have the alignment cylinder attached to its distal end, and the linear stage can be used to adjust the location of the clamping fixture until the mating cylinder mates with the notch pattern of the top surface of the clamping fixture. This verification method is accurate to the precision of the 3D printer used which in our case is on the order of 100 m.

3.2.2 Testing Protocol

With a specimen mounted in place and aligned with the machine, the linear actuator is brought down until a compressive preload of 5 N is detected, at which time the position measurement is zeroed out. The push-out rod is then displaced downward at a constant rate of 5 mm/min (0.0083 mm/s) until the region of interest is completely extruded from the bone. Displacement rate was

determined following Spicer, et al. [36] . Additional details of the protocol are provided in the Appendix.

For device validation, push-out tests were first performed with explanted rat cranial caps (N = 30). This study was approved by the Texas A&M University IACUC (AUP 2016-0348). Fischer rats (N = 60, male, 8 weeks old) were each induced with non-critically sized, bilateral cranial defects (5 mm nominal diameter). For each animal, the second likewise treated defect site was reserved for other testing, thereby yielding a total of 30 treated cranial caps for push-out tests. Rats (N = 12) were treated with an autograft (i.e., the excised bone flap), yielding 6 specimens for push-out testing. Another group of rats (N = 48) were treated with a novel self-fitting shape memory polymer (SMP) scaffold (d 5.5 mm x t 1.5 mm), yielding 24 specimens for push-out testing. The SMP scaffolds permitted press-fitting into defects, wherein shape recovery following exposure to warm saline (T 55 žC) promoted scaffold expansion to the perimeter. Scaffolds were prepared as semi-interpenetrating networks (semi-IPNs) with crosslinked poly(-caprolactone)-diacrylate (PCL-DA, Mn 10k g/mol) and poly(L-lactic acid) (PLLA, Mn 15k g/mol) at a 75:25 wt% as previously reported. [38] Such scaffolds have been shown to exhibit interconnected pores (average size of 220 m) and a compressive modulus of 23.8 MPa. All scaffolds were prepared with a cell adhesive peptide (RGD; 1 mM) and half of the scaffold specimens were coated with a bioactive polydopamine as previously reported. [39] Yielding 6 push-out test specimens each, defects were treated with (i) uncoated scaffolds, (ii) uncoated scaffolds pre-seeded with rat-derived bone marrow mesenchymal stem cells. [39, 40] (BMSCs; 35k), (iii) coated scaffolds, and (iv) coated scaffolds pre-seeded cells. Scaffolds were sterilized via EtO prior to implantation. For both groups of rats (i.e., autograft- and scaffold-treated), studies were terminated after 4 weeks. Calvaria were removed using a dremel diamond wheel and wrapped in an isotonic saline or 0.9% saline soaked gauze sponges, placed in specimen bags, and placed in a -20 žC freezer until testing. To validate design versatility, push-out tests were also performed on rabbit calvaria with the geometrical parameters of the clamp scaled appropriately. This study was approved by the Texas A&M University IACUC (AUP 2015-0240/2018-0403). New Zealand White rabbits (N

= 2, male, 6 months old) were induced with non-critically sized, bilateral cranial defects (8 mm nominal diameter). Each animal was treated with one SMP scaffold (d 9 mm x t 2 mm) and one polyetheretherketone (PEEK) implant (d 8.5 mm x t 2 mm). The scaffolds were prepared from PCL-DA (Mn 10k g/mol) per prior reports. [38, 41] Scaffolds exhibited interconnected pores (average size of 220 m) and a compressive modulus of 18.0 MPa. Scaffolds were sterilized via gamma irradiation and the PEEK specimens were sterilized via EtO. The study was terminated after 16 weeks. Calvaria were removed as above. The design was further validated with push-out tests performed on another group of rat cranial caps (N = 24). This study was approved by the Texas A&M University IACUC (AUP 2019-0447). Fischer rats (N = 24, male, 8 weeks old) were each induced with a critically sized, unilateral cranial defect (8 mm nominal diameter). Rats (N = 8) were treated with an autograft (i.e., the excised bone flap). The remaining rats (N = 16) were divided equally into two groups treated by an SMP scaffold: (i) a PCL-DA/PLLA semi-IPN scaffold (d 8.6 mm x t 2 mm) (analogous to that noted above), and (ii) a PCL/polydimethylsiloxane (PDMS) scaffold (d 8.6 mm x t 2 mm). As per a prior report, the PCL/PDMS scaffolds were prepared as a co-network with PCL-DA (Mn 10k g/mol) and PDMS-dimethacrylate (PDMS-DMA; Mn 5k g/mol) at a 75:25 wt% ratio. [42] Such PCL/PDMS scaffolds have been shown to exhibit interconnected pores (average size of 230 m) and a compressive modulus of 5 MPa. to All scaffolds were prepared with a cell adhesive peptide (RGD; 1 mM) and sterilized via EtO. The study was terminated after 12 weeks. Calvaria were removed as above.

3.3 RESULTS

3.3.1 Rabbit Results

For the rabbit calvarial models, the scaffolds were implanted into right calvarial defects, and left calvarial defects were each treated with a PEEK disc. Push-out tests were performed at 16 weeks. The pre-implantation modulus of the PEEK implants (E = 220 $\pm$ 19.0 MPa) was orders of magnitude higher than that of the SMP scaffold (E 20 MPa). Yet, the partially healed defects treated with SMP scaffolds were noticeably more resistant to pushout than the contralateral PEEK

implants in terms of both the maximum load required (Figure 3.8a) and stiffness (Figure 3.8b). This is attributed to the favorable bone tissue ingrowth at the scaffold/defect perimeter, as confirmed histologically and by micro-CT by our collaborators. Differences in failure load and stiffness were calculated for each rabbit as the value of the SMP scaffold treatment minus the value of the PEEK treatment (Table S3 and Table S4). A Students paired t-test performed on both the failure load (μ = 85.7, σ= 2.90, p = 0.0152) and the stiffness (μ= 85.3, σ= 5.94, p = 0.0313) showed the measured differences to be statistically significant. The porous SMP scaffolds likely surpassed the solid PEEK controls biomechanically due to tissue ingrowth especially at the perimeter, consistent with the histological and micro-CT findings of our collaborators. Moreover, these findings support the notion that the self-fitting SMP scaffold offer clinical advantages for treatment of CMF defects due to improved osseointegration. [43]

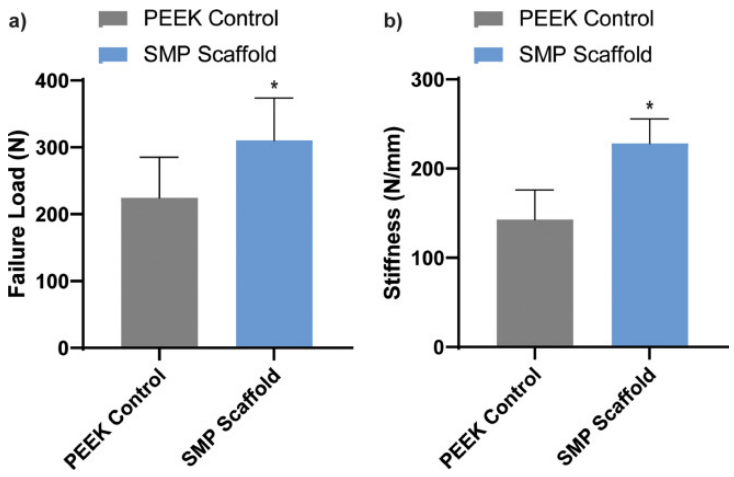

Figure 3.8: (a) Failure load and (b) stiffness determined via biomechanical push-out tests, *p < 0.05.

3.3.2 Rat Results

For the rat samples, two variants of the SMP were made, Scaffold A: (PCL/PLLA 75/25) and Scaffold B: (PCL-DA/PDMS-MA 75/25). Forty-eight (48) rats were induced with bilateral cranial defects 5.5 mm diameter, then subdivided into 8 treatment groups (n=6), and sacrificed 4 weeks

post implantation. The treatment groups varied whether or not the scaffolds were coated with bioactive polydopamine and whether or not they were treated with bone-derived mesenchymal stem cells (BMSCs); "low cells" denotes treatment groups seeded with 35,000 BMSCs and "high cells" denotes treatment groups seeded with 4 million cells. The max load for each of the treatment groups are tabulated below in **??** One rat sample (Uncoated-B, no cells) was excluded. The bone flap treatment showed the lowest average failure load, significantly lower than Uncoated-A no cells ($p = 0.029 < 0.05$) and Coated-A no cells ($p = 0.049 < 0.05$). No significant differences were found between any other groups. (Figure 3.9

Table 3.1: Failure load of murine samples under various biological treatments.

Treatment	Avg Failure Load (N)	Stdev
Autograft Bone Flap (control)	114.60	49.47
Uncoated-A, No cells*	174.97	57.20
Coated-A, No cells*	171.41	40.64
Uncoated-A, Low cells	171.11	58.17
Coated-A, Low cells	146.38	43.27
Uncoated-B, No cells	150.48	29.09
Uncoated-B, High cells	130.43	31.29
Uncoated-A, High cells	142.44	36.54

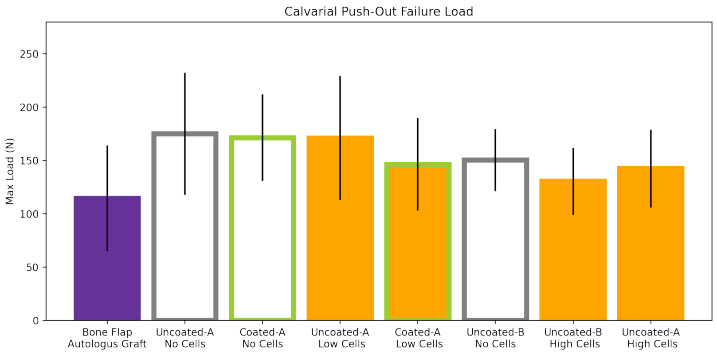

Figure 3.9: Failure load determined via biomechanical push-out tests.

3.4 DISCUSSION

The method described herein has demonstrated several important benefits for push-out testing of calvarial defect specimens. Firstly, the circumferential clamping modality significantly reduced the bending induced in the cranial cap as compared to lateral compression clamps. Secondly, having a clamp that is easily removed from the testing machine allows visual inspection of specimen alignment in the clamp that is not possible with other designs. Thirdly, the targeted notch pattern ensures the defect, push-out rod, and through-hole are reliably coaxial to sub-millimeter precision. Lastly, 3D printing allows each sample to have its own, inexpensive clamp; this was found to be a significant advantage to improve workflow efficiency. This permitted each sample to be aligned and secured in an individual clamping fixture and then store the clamped specimen in a warm (37 °C) saline bath until ready for testing. This also helped maintain tissue hydration by reducing exposure time to air. Additionally, the reported method translates particularly well to the use of bilateral calvarial defects which are favored to increasing study power while decreasing animal usage. While bilateral defect models are common for histological studies, their use in push-out and other biomechanical studies is rare due in part to the above mentioned geometrical difficulties of laterally located defects. Our method addresses these difficulties, thus allowing the benefits of bilateral models to translate to the mechanical evaluation of calvarial defect repair devices.

Despite these advantages to this method, several limitations are noted. First, the clamping bolts are independently tightened which may result in non-uniformity of clamping force and non-defined effects. In this study, a single researcher secured the samples in place after developing proficiency in the method using several pilot samples. In future work, a second iteration will use a single thread to apply the clamping force along the common central axis. A second limitation of this method is the necessity for sufficiently thin or translucent test articles to verify defect alignment with light that may prohibit utility for calvarial push-out tests of larger animal models or other push-out applications (e.g., dental or long-bone). Furthermore, the geometry and material (ABS) have only been validated at relatively small loads (i.e., < 250 N). Given its high compressive modulus, ABS can withstand much higher compressive loads; however, the 80% print infill sufficient for

the present experiment may not be sufficient for higher load applications. While the design could be translated into a different material (e.g., stainless steel), there may be a trade-off in cost and efficiency. A third limitation is the visibility of the experiment. If the push-out rod were visible throughout the entirety of the experiment, the initial contact with the sample could be visually verified, interference with the interior of the through-hole could be detected, and the failure mode of the test article could be analyzed in more detail. Finally, the z-axis on the Newport linear stage was unnecessary as the linear actuator controls the push-out rod's position; in later iterations of this method, we removed the z-axis stage and used x-y linear stages only.

The data and results herein presented confirm that the SMP mechanical performance is comparable and occasionally superior to that of the gold standard autologous bone graft. Interestingly, the high seeded treatments all showed a (non-significant) average lower push out force than the low seeded groups. These groups should be cross-checked with the histology results to compare the degree of osteointegration. The statistical significance of the "Uncoated-A no cells" ($p = 0.029$) and "Coated-A no cells" ($p = 0.049$) groups should not be over-interpreted. Each of the 12 defects in the treatment groups is treated as an independent data point in the present analysis. While there is precedent in the relevant literature for this approach. [44], technically this is not correct; 2 measurements x 6 rats is not equivalent to 1 measurement x 12 rats. Because the bilateral defects were treated with the same repair, it violates the independence assumption because each rat is producing two data points in the same treatment group. Since this sample dependence is not easily accounted for, the more conservative interpretation is that all SMPs had "comparable mechanical performance" to the autografts at the 4 week time point.

3.5 CONCLUSION

A novel, standardized method has been developed for evaluating the push-out performance of CMF repair techniques in small animal models; this method is scalable as validated by use in bilateral and unilateral defects in both leoprine and murine models. The novel shape memory polymer investigated by this new method has demonstrated comparable (and somewhat superior) mechanical performance in comparison to the gold standard autologous bone graft. Given its

other advantages, such as ease of manufacture and surgical installation, the SMP is a promising alternative for CMF defect repair.

4. BIOMECHANICAL ASSESSMENT OF CEMENTLESS THR BROACH DESIGN: EFFECT ON BROACHING, STEM INSERTION, AND SUBSIDENCE

This content in this chapter in an advanced preparation paper tentatively titled *Quasi-static assessment of three cementless THR broach designs: effect on broaching, stem insertion, and subsidence in simulated healthy and sclerotic cancellous bone*. Author List: Zachary T. Lawson, B.S., Danielle Hollenbeck, DVM, Catrina J. Silveira, DVM, M.S., Michael R. Moreno, PhD, Andrew B. Robbins, PhD, W. Brian Saunders, DVM, PhD, DACVS

4.1 INTRODUCTION

Total hip replacement (THR) is a highly-successful treatment for pathologies of the canine hip such as hip dysplasia, femoral head or neck fracture, acetabular fracture, Legg-Calve-Perthes disease, or traumatic hip luxation. [45, 46, 47, 48] While cemented THR was the standard of care for decades, press-fit (i.e. cementless) implants were subsequently developed and are now predominantly utilized for the majority of canine THR patient. [45, 46, 47] Cementless THR systems rely on a precision preparation and implantation technique in which the implant and adjacent bone are in uniform contact along the entire implant surface. Initial implant stability is provided by friction between implant and bone, whereas long term stability occurs via bone ongrowth and ingrowth. [45, 46, 47, 48]

While technique and instrumentation vary across implant systems, cementless femoral canal preparation is typically performed using a series of femoral broaches. Femoral broaches match the dimensions of cementless stems and contain teeth that crush and remove adjacent cancellous bone during impact insertion. Successful femoral broaching involves impaction of the femoral broaches along the anatomic axis of the femur, with broach alignment parallel to the proximal endosteal surfaces in both frontal and sagittal planes. Completion of the broaching process is guided by preoperative templating as well as recognition of increasing broaching resistance by the surgeon.

Despite the high clinical success rate reported with modern cementless THR systems, com-

plications related to femoral broaching can occur. Two common complications associated with broaching are broach malalignment and insertion of an excessively large broach, both of which result in femur fracture. Fissure fractures are addressed by cerclage fixation followed by placement of a cementless or cemented stem, or alternatively conversion to femoral head and neck ostectomy (FHO).[46, 47] In some canine THR candidates, the cancellous bone of the proximal femur experiences an increase in mineral deposition in response to alterations in loading of the proximal femur.[49, 50] This finding is identified as increased bone opacity on pre-operative radiographs and is termed proximal femoral sclerosis. In this sub-population of dogs, the tooth design of existing THR broaches is insufficient to crush or cut the sclerotic bone. The clinical result is prolonged broaching and an increased risk of intraoperative femur fracture. [45] Regrettably, development of broaches with design features tailored to sclerotic bone has not been a focus for the field. The current crushing tooth design used for one common canine cementless THR system has remained unchanged since 2005.

Another complication associated with femoral broaching is deviant broach installation leading to an insufficient press-fit envelope. Imprecise broaching is a more insidious complication as it is often not recognized during surgery; however, it results in loss of press-fit and stem subsidence in the early postoperative period. Stem subsidence has various consequences, including subsidence and bone ingrowth (stable stem with a reduced working neck length), subsidence and fibrous ingrowth, and in extreme cases subsidence leading to femur fracture and/or prosthesis luxation. Modified cementless stems have been developed to reduce the incidence of subsidence, but their placement is predicated on proper press-fit technique. [45]

Given the broaching complications described above, there is a need for additional cementless broaches designed to efficiently and safely prepare sclerotic femoral bone. Importantly, the consequences of novel broach designs on stem insertion and subsidence must also be considered. Therefore, the objective of this study was to develop novel cementless broach designs and evaluate their biomechanical performance during broaching, stem insertion, and stem subsidence, in simulated typical and sclerotic cancellous bone.

4.2 METHODS

4.2.1 Broach design and fabrication

Broaches were designed and fabricated by Biomedtrix (Whippany, NJ, USA) using manufacturing processes similar to commercially available BFX™ broaches. Size 8 broaches were selected for investigation in the present study (n=3 broaches/group) due to the frequency with which these broaches are used in clinical cases. The control broach was the BFX™ design that has been in use since circa 2005 (Fig 4.1A). This design contains compaction (i.e. crushing) teeth to compact cancellous bone and produce bone densification at the margin of the femoral preparation. [51] Test Group 1 (TG1) was designed with identical tooth pitch, chip chamber depth, and rake angle to control broaches, with the addition of cutting flutes to the cranial, lateral, and caudal surface of the broach (Fig 4.1B). Test Group 2 (TG2) was designed with novel sharp extraction teeth with unique tooth pitch, chip chamber depth, rake angle, and tooth pattern (Fig 4.1C). TG2 was designed with the goal of providing a sharper cutting tooth capable of cutting sclerotic cancellous bone while generating a more precise external envelope. External dimensions of all broaches were identical. All broaches were inspected to confirm clinical manufacturing tolerances were achieved. The shaft of each broach was externally threaded (1/4"-20) to interface with R.T.S. testing fixtures.

4.2.2 Selection and initial preparation of bone analogues

Solid rigid polyurethane foam blocks (130 mm high x 80 mm long x 40 mm wide) were acquired from a commercial vendor (Sawbones, Vashon Island, Washington, USA). Two foam densities were selected in order to simulate two densities of cancellous bone. The 15 pounds per cubic foot (pcf) foam (product #1522-02) was selected to simulate material properties of typical canine cancellous bone. The 25 pcf foam (product #1522-660) was selected to simulate material properties of dense cancellous bone associated with proximal femoral sclerosis. [52, 53] Stock polyurethane blocks were first modified with a 45°chamfer cut to generate a surface analogous to the femoral neck ostectomy (Fig 4.2). Blocks were then sub-sectioned into individual test blocks (130 mm high x 29 mm long x 40 mm wide). A 5 mm diameter channel was drilled through the

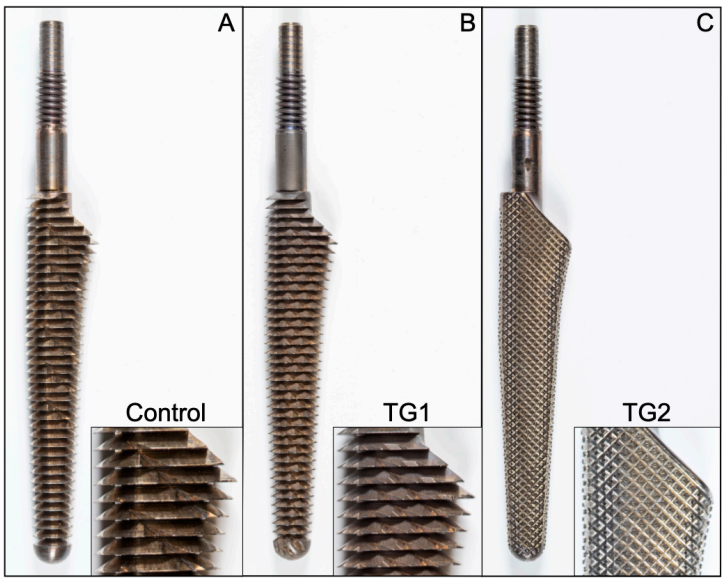

Figure 4.1: Three tooth designs: Control (A), Test Group 1 (B), and Test Group 2 (C).

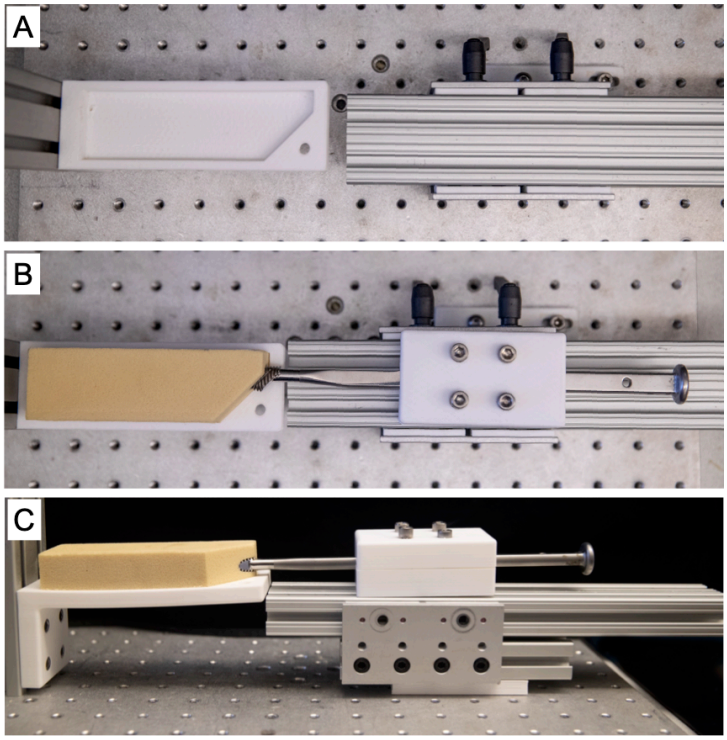

Figure 4.2: Custom prepping setup made of 8020 and 3D printed components. Top empty (A), Top with broach and block sample (B), Side view (C).

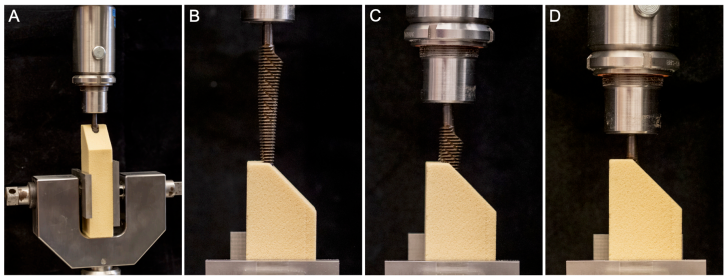

Figure 4.3: Installation of the broach from contact to full insertion (D)

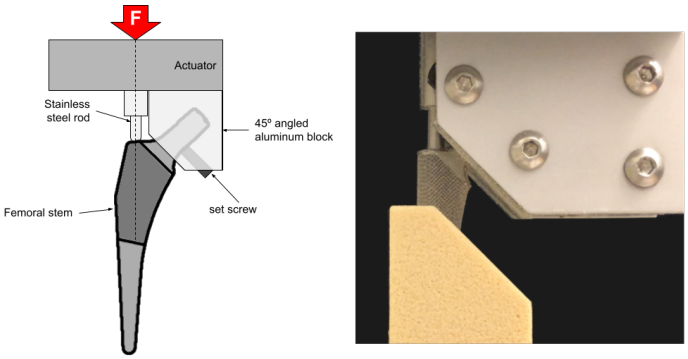

Figure 4.4: Apparatus for installing and extracting the femoral stem.

long axis of each block, centered 12.7 mm from the shoulder of each block. Each channel was sequentially enlarged in 1 mm increments to a final diameter of 8 mm.

Prior to biomechanical testing, femoral preparation was performed on each test block to mimic BFX^{TM} workflow for clinical cases. Blocks were placed in a custom preparation device composed of an aluminum breadboard base (#MB1218U Thorlabs, Inc, Newton, NJ, USA Model) with a custom-designed, 3D printed Polylactic Acid (PLA) test block fixture on one end (Fig 4.2). The 3D printed holder served to secure each test block and align the long-axis of the previously established 8 mm diameter channel with a linear bearing (#6733, 80/20 Inc, Columbia City, IN, USA) fixture centered with the channel. A size 7 fluted reamer was centered on the 8 mm channel and inserted

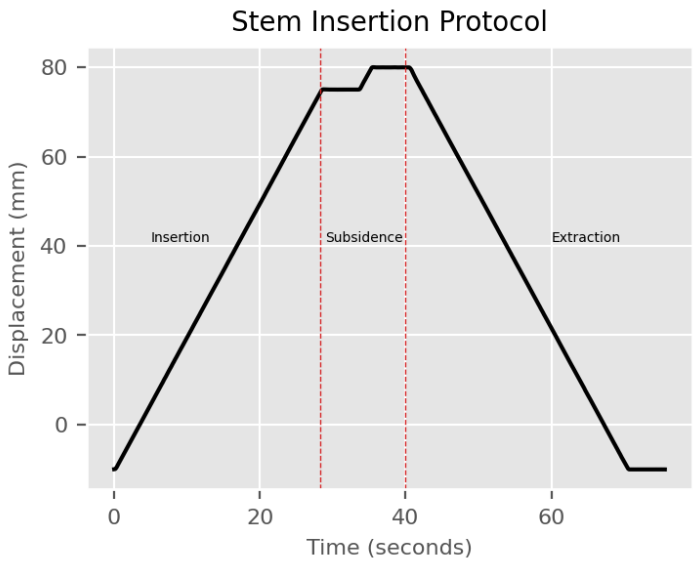

Figure 4.5: Protocol for stem insertion, subsidence, and extraction.

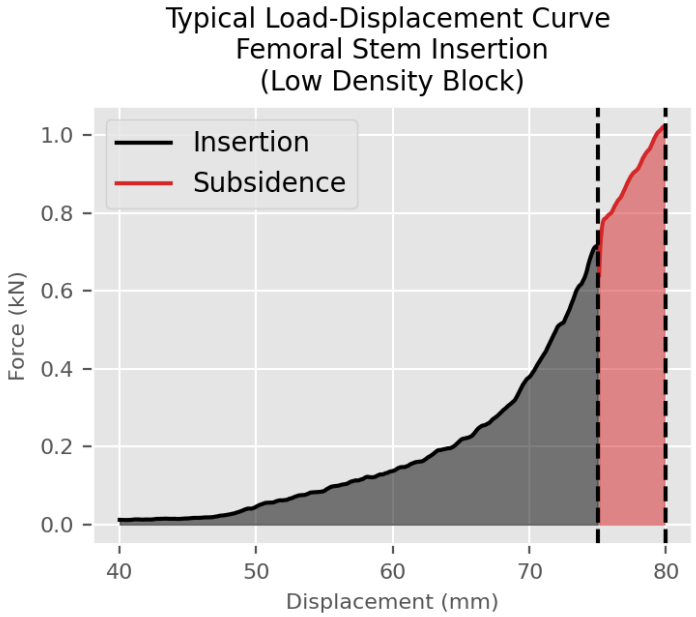

Figure 4.6: Typical load-displacement during femoral stem test.

under power until the reamer was seated with the 3/4 reamer line flush with the simulated neck cut. BFX^{TM} broaches were then secured within a custom-designed 3D printed broach handle fixture

and inserted in ascending order using a BFX^{TM} THR mallet until the shoulder of the broach was flush with the simulated neck cut. The 7 BFX^{TM} broach was the final broach used to complete the test block preparation.

4.2.3 Broach testing procedure

Prepared test blocks were secured in a materials testing machine equipped with a linear actuator (Thompson Linear, Inc., Radford, VA, USA) for quasi-static broach insertion and removal. Blocks were secured with stainless steel clamps to align each test block preparation bed with the central axis of the actuator. Individual test broaches (Control, TG1, TG2) were secured to the actuator by the threaded end and allowed to rotate freely to self-align during insertion into the test blocks (Fig 4.3). Full insertion was defined as 75 mm, corresponding to the length of a complete set of cutting teeth for the 8 BFX^{TM} broach. In an attempt to simulate the clinical scenario of sequential broach insertion, removal, and cleaning, loading was performed in a series of five drives, each followed by extraction at a constant rate of 3 mm/sec. Each drive started at 0 mm then advanced a pre-established distance to mimic the clinical broaching process. Debris from the test block was cleaned from the broach during each extraction. Load and displacement were measured with a 500 lbf load cell (Futek, Inc., Irvine, CA, USA) a 15 in. stroke LVDT (TransTek, Inc., Ellington, CT, USA), respectively. The peak load for each drive was reported and energy required to insert the broach was calculated via a work energy integral. Cumulative energy was calculated by summing the drive energy across all five drives.

4.2.4 Femoral stem insertion and subsidence testing procedure

To approximate the clinical performance of each broach, a #8 electron beam melted (EBM)-BFX^{TM} femoral stem (BioMedtrix, Inc.) was inserted into the broached test blocks using a custom fixture connected to the linear actuator. The custom fixture consisted of a round tip stainless steel rod coaxial with the linear actuator which mated with the drive divot of the femoral stem, ensuring the applied compressive force was coaxial with the stem. Two 45°flat joining plates (#4145, 8020 Inc.) and additional aluminum extrusion components were combined to create an

angled bracket that attached to the stem neck. The stem was allowed to rotate freely about the neck axis until positioned in place by mating the drive divot to the stainless steel hemispherical rod. Once in place, the stem alignment with the actuator axis was verified with a digital protractor (Pro360, Inc.), then fixed in place with a set screw perpendicular to the stem neck (Fig 4.4). A small pre-stress was introduced into the apparatus by tightening the connection of the rod to the actuator with a nut; this pre-stressing ensured compressive force from the actuator was transmitted along the loading axis of the stem during insertion + subsidence and tensile force was transmitted on the neck of the stem during extraction. Measurement error introduced by pre-stressing was determined to be insignificant due to the small magnitude and consistent application across all samples. Comparative inferences are not influenced; moreover, ensuring coaxial loading across all samples is a more significant design consideration. Free rotation about the loading axis was permitted for the entire apparatus to allow the stem to self-align with the preparation bed of each test block (Fig 4.4), as was the case with the broach installation.

Insertion proceeded at a rate of 3 mm/s for a distance of 75 mm such that the proximal aspect of the stem was flush with the simulated neck cut. After a five second hold, the stem was driven an additional 5 mm at 3 mm/s to simulate stem subsidence in the early post-operative period. Upon the completion of each test, the BFX stem was extracted from the test block at 3 mm/s then cleaned with a nylon brush and compressed air to remove accumulated foam block debris (Fig 4.5). To minimize the effect of stem re-use, a representative sample (n=3) of the broached test blocks were used for each broach design for both test block density and the order in which test blocks were evaluated was randomized. Peak force and cumulative energy were calculated for both insertion and subsidence regimes as a proxy for stem stability, i.e., resistance to subsidence (Fig 4.6).

4.2.5 Statistical analysis

All datasets were examined for normality using Kolmogorov-Smirnov Test of Normality. Peak load/force and cumulative energy for broach insertion were analyzed using one-way ANOVA followed by Tukey HSD. Peak force (kN) and cumulative energy (J) were analyzed using one-way ANOVA with Tukey HSD post-hoc analysis for stem insertion and subsidence data. Python 3.7

(Python Software Foundation, Beaverton , OR) was used for all data analysis. Significance was assumed at p 0.05.

4.3 RESULTS

4.3.1 Broaching results

For the 15pcf test blocks simulating typical cancellous bone, TG1 required the least cumulative energy at 10.76 (±0.29) J, followed by Control at 12.18 (±1.20) J and TG2 at 16.66 (±0.78) J (Figs. 4.9 and 4.10). All groups were significantly different from each other (p<0.01). For the 25 pcf test blocks simulating more sclerotic cancellous bone, TG1 broaches required 32.60 (±2.54) J, Control broaches required 33.25 (±2.16) J, and TG2 broaches required 59.97 (±3.07) J (Figs. 4.9 and 4.10). A difference between the performance of Control and TG1 broaches was not detected (p = 0.75). There was a difference between TG2 and both Control and TG1 (p<0.01). Collectively, these data indicate that Control and TG1 broaches require lower energy for sequential broach insertion regardless of foam block density, with TG1 broaches exhibiting the lowest insertion energy.

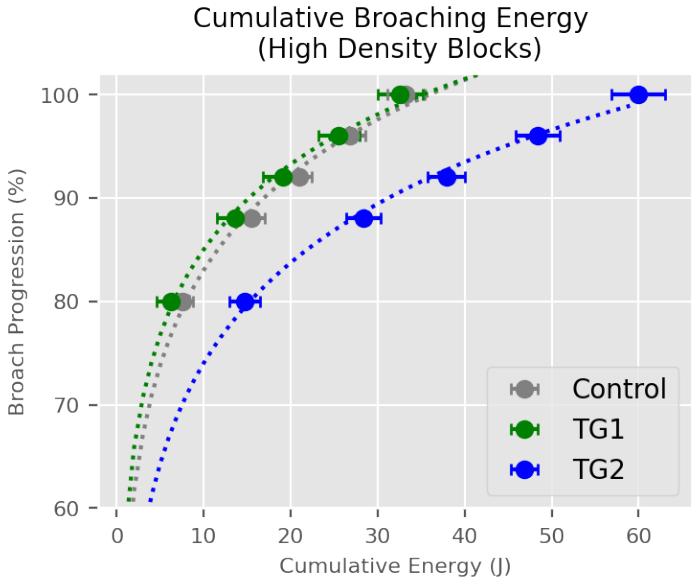

Figure 4.7: Cumulative energy at each drive.

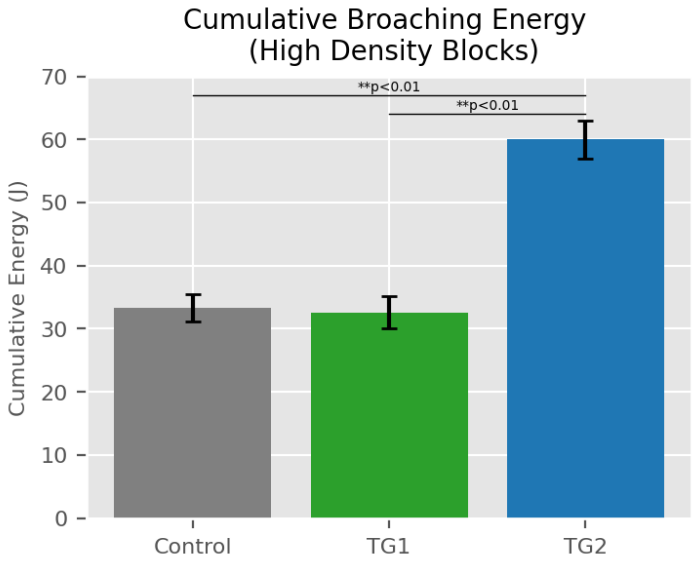

Figure 4.8: Cumulative energy for entire broaching process.

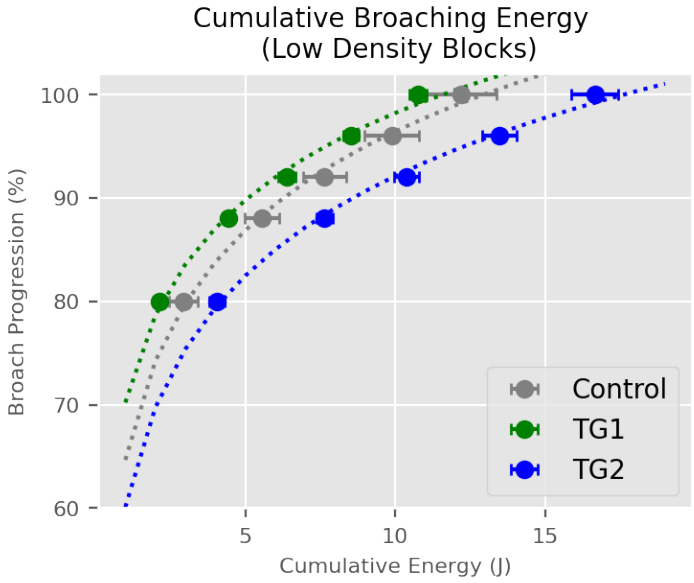

Figure 4.9: Cumulative energy at each drive.

4.3.2 Femoral stem insertion and subsidence results

For the 15 pcf test blocks, energy required for stem insertion for Control, TG1, and TG2 were 4.90 (± 0.08) J, 6.30 (± 0.95) J, and 5.88 (±1.01) J, respectively. Energy required for 5 mm

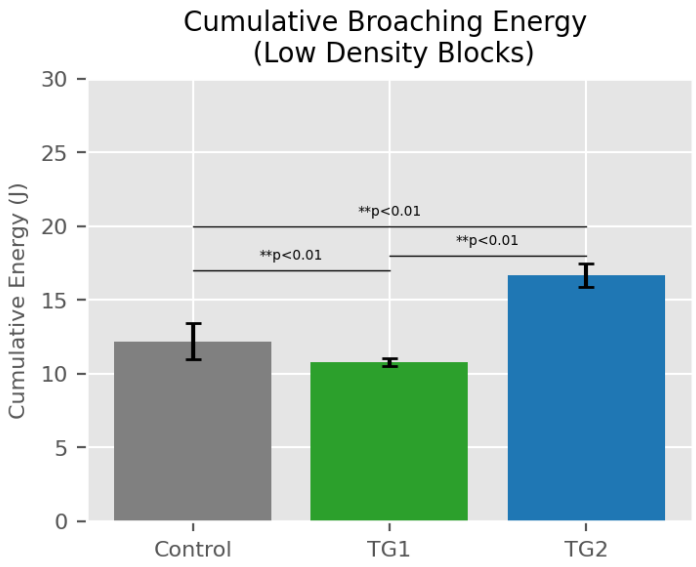

Figure 4.10: Cumulative energy for entire broaching process

subsidence for Control, TG1, and TG2 were 3.54 (±0.07) J, 4.20 (±0.37) J, and 3.84 (±0.46) J, respectively. Cumulative energy for insertion and subsidence are provided in Figs. 4.11 and 4.12. Differences between these values were insignificant ($p > 0.20$).

For the 25 pcf test blocks, the average work energy to insert the stem into a block prepared with Control broaches was 14.53 (± 0.81 SD) J, lower than TG1 prepped blocks, 22.53 (± 1.04 SD) J ($p<0.01$), and TG2 prepped blocks, 19.38 (± 3.00 SD) J ($p<0.05$). A significant difference was not detected between TG1 and TG2 ($p=0.25$). During implantation, the TG1 prepped blocks showed the highest average peak load of 2.69 (± 0.90 SD) kN, significantly more than both Control, 2.04 (± 0.31 SD) kN ($p<0.01$), and TG2, 2.23 (± 1.86 SD) kN ($p<0.05$). No significant difference was found between the Control and TG2 ($p=0.09$). Interestingly, the TG1 prepped blocks required 14.49 (± 0.49) J to subside 5 mm, which was significantly more than blocks prepared with Control [11.09 (±0.09) J, $p<0.01$] or TG2 [12.57 (± 0.81) J, $p<0.05$] broaches. Cumulative energy for insertion and subsidence are provided in Figs 4.13 and 4.14. Collectively, these data suggest that femoral test blocks prepared with TG1 and TG2 broaches required more work energy for stem insertion and subsidence, with TG1 prepared blocks exhibiting the most resistance during stem

insertion and subsidence.

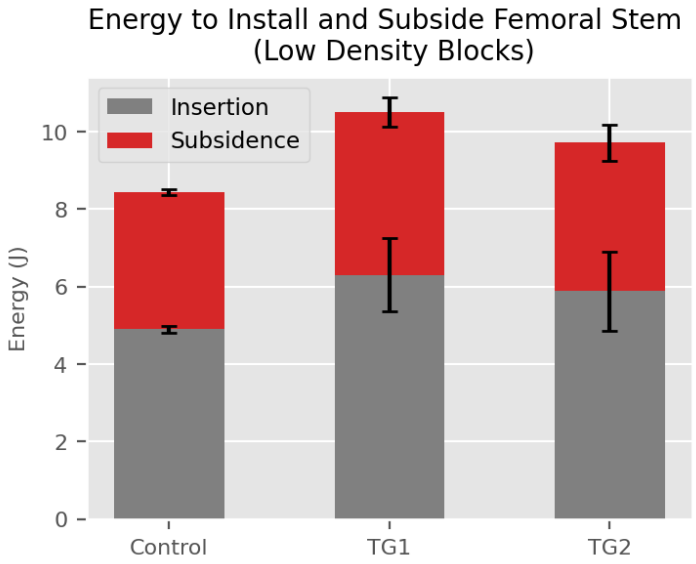

Figure 4.11: Energy needed to subside the femoral stem.

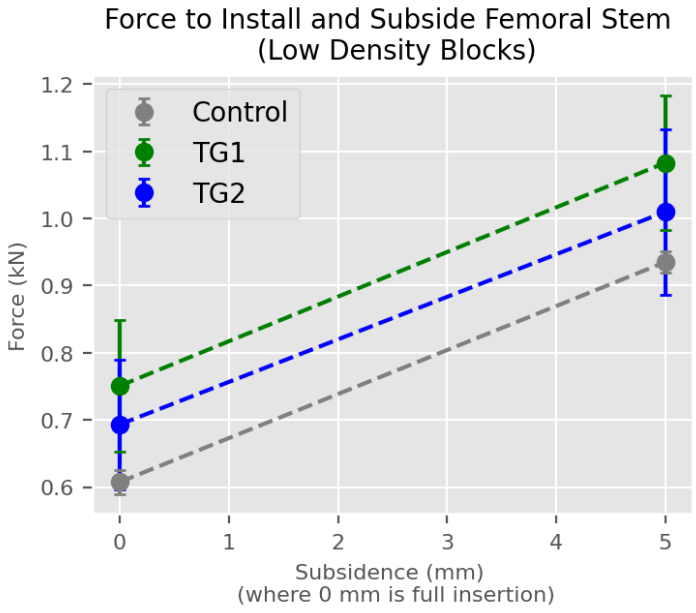

Figure 4.12: Force needed to subside the femoral stem.

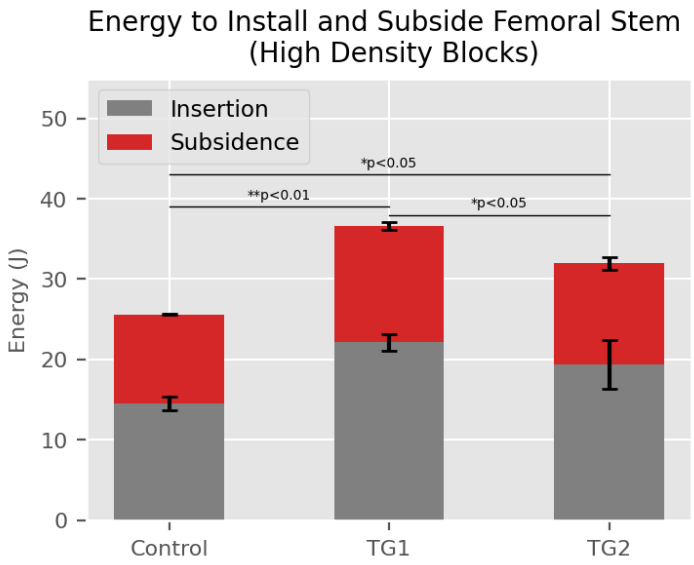

Figure 4.13: Energy needed to subside the femoral stem.

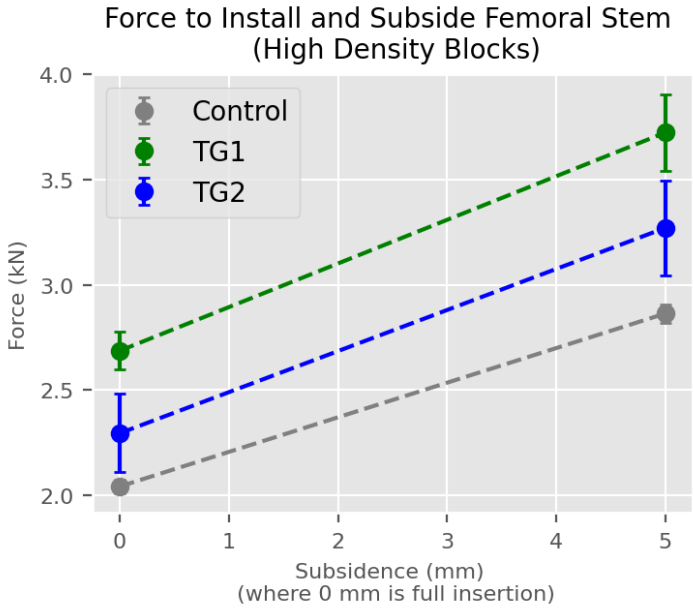

Figure 4.14: Force needed to subside the femoral stem.

4.4 DISCUSSION

This study set out to mechanically evaluate the cutting efficiency of three different broach designs in 15 pcf and 25 pcf polyurethane foam intended to simulate typical and sclerotic bone, respectively. Subsequent to the broaching, a femoral stem was inserted and subsided to evaluate the envelope prepared by each of the broaches. TG1 required/exhibited lower energy for broaching in both foam densities and additionally when stems were inserted into TG1 prepared blocks, loads for stem insertion and subsidence were the highest for TG1 broaches. However, the TG1 broach afforded an average 18.7% (low density blocks) to 30.6% (high density blocks) greater subsidence resistance when compared to Control broaches. One potential explanation for these findings are the cross sectional area/pattern of the TG1 broaches compared to the BFX^{TM} stem contour/shape. Vertical ridges were visually observed in the preparation beds of the samples broached by the TG1 design; it is likely these were due to the additional sets of vertical grooves in the TG1 tooth design. Thus, the lower work energy could be explained by the fact that the volume of cut material is slightly less than the Control. Secondly, the increased stem stability could be attributable to these ridges being crushed by the stem during insertion. Overall, these results suggest the use of a final broach composed of the TG1 tooth design might be useful in the clinical setting to resist subsidence.

Interestingly, TG2 broaches were designed with sharp teeth for enhanced cutting of bone typical and dense cancellous bone. However, the TG2 exhibited the highest amount of energy for broach insertion for both test block densities. In stem insertion and subsidence testing, TG2 prepared blocks exhibited improved performance as compared to Control test blocks, but were inferior to TG1 prepared test blocks. One explanation for these results is related to the low profile cutting teeth on TG2, referred to as the chip chamber depth. Chamber depth for TG2 broaches was smaller than Control and TG1 broach designs. It is likely that this design led to rapid teeth filling with foam debris. Theoretically, the lower profile of TG2 broaches would provide for a tighter tolerance envelope in the bone, however the results of the present study are in contrast to this concept.

4.4.1 Limitations

As with all studies, this study is not without limitations. One significant limitation preventing direct translation to the clinical setting is the quasi-static testing methodology. Clinically, broaches and stems are inserted by repeated striking with a mallet. Such impact loading is significantly different from the quasi-static methods used in the present study. Non-impact tests are routinely used as an initial evaluation of broach cutting efficiency in clinical applications. [54] in part because non-clinical mechanical broaching is nearly universally conducted non-impact. [55, 56, 57, 58] To bridge this gap, future work will expand upon the present study by developing an impact model for evaluation of canine cementless THR broaches. These work is currently in progress.

Another limitation is the selection of polyurethane foam bone substitutes for biomechanical testing. As has been extensively documented in the literature, foam analogues are useful approximations of bone, but are significantly different in several ways. [59, 60] For example, bone is hydrated, viscoelastic, anisotropic material. The proximal femur is a complex geometric structure composed of cortical and cancellous bone and an elegant microstructural trabecular design. This complex structure cannot be simulated by foam blocks; moreover, these material properties are likely to exacerbate the mechanical difference in impact regimes. However, it is standard practice to use these bone substitutes for exploratory work such as the present study. Per Hausmann . [59], the ideal study design supplements the results from analogues with results from cadaveric studies; future work aims to culminate in a cadaveric evaluation following broach redesign incorporating the findings from the present quasi-static and future impact testing.

Due to these limitations, the translation from this study to clinical application should be tempered due to the material differences of the bone simulant and loading regime.

4.5 CONCLUSION

This study set out to mechanically evaluate the cutting efficiency of three different broach designs in 15 pcf and 25 pcf polyurethane foam intended to simulate typical and sclerotic bone, respectively. Subsequent to the broaching, a femoral stem was inserted and subsided to evaluate

the envelope prepared by each of the broaches. The novel low-profile teeth design (TG2) exhibited the worst performance, indicating a move in the wrong direction with respect to the clinical desire to reduce the incidence of femoral fissure during broaching. The modified vertical groove design (TG1) exhibited a slight superior performance with respect to ease of broaching and stability of stem installation. Improved performance may be attributable to the vertical ridges created along the vertical axis of the preparation bed, resulting in less foam volume broached and additional material crushed by the stem during installation. While the procedure and results herein represents a standard evaluation of broach cutting efficiency, direct translation to clinical application should be cautioned. In addition to the well-known significant material differences between polyurethane SawBones blocks and living bone, the quasi-static loading modality employed differs from the clinical environment wherein the broach is installed by repeated mallet impacts. Undoubtedly, the peak loads exhibited in this study underestimate the peak loads experienced in impact. To this end, future work is underway to develop an impact testing set up and procedure to better approximate the clinical loading environment.

5. SUMMARY

The work herein contains three biomechanical experiments conducted in the field of orthopedic biomechanics.

First a novel double tension slide suturing technique (DTS) was mechanically evaluated in a cadaveric study. The DTS technique demonstrated a greater, but similar load to failure as the gold standard tension slide technique; thus, the redundancy provided by the second suture has an inherent advantage without compromising the biomechanical performance. The DTS technique maintains the many potential advantages to the tension slide technique without the risk of bone tunnel fracture with an interference screw. Furthermore, the redundancy of a second suture should provide a failsafe if either strand of the initial sutures was damaged by the needle, abrasion against the bone, or loss of knot security at the button. By passing 2 sutures through the tendon, the present technique increases the cross-sectional area of tendon in contact with suture to reduce the force transmitted through the individual passes of the suture and reduce failure at the tendon-suture interface.

Second, a novel, standardized method was developed for evaluating the push-out performance of cranio-maxillofacial (CMF) repair techniques in small animal models; the method is scalable as validated by use in bilateral and unilateral defects in both leoprine and murine models. The novel shape memory polymer investigated by this new method demonstrated comparable (and somewhat superior) mechanical performance in comparison to the gold standard autologous bone graft. Given its other advantages, such as ease of manufacture and surgical installation, the SMP is a promising alternative for CMF defect repair.

Third, three different broach designs were mechanically evaluated in 15 pcf and 25 pcf polyurethane foam intended to simulate typical and sclerotic bone, respectively. Subsequent to the broaching, a femoral stem was inserted and subsided to evaluate the envelope prepared by each of the broaches. The novel low-profile teeth design exhibited the worst performance, indicating a move in the wrong direction with respect to the clinical desire to reduce the incidence of femoral fissure during broach-

ing. The modified vertical groove design exhibited a slight superior performance with respect to ease of broaching and stability of stem installation. Improved performance may be attributable to the vertical ridges created along the vertical axis of the preparation bed, resulting in less foam volume broached and additional material crushed by the stem during installation. While the procedure and results herein represents a standard evaluation of broach cutting efficiency, direct translation to clinical application should be cautioned. In addition to the well-known significant material differences between polyurethane SawBones blocks and living bone, the quasi-static loading modality employed differs from the clinical environment wherein the broach is installed by repeated mallet impacts. Undoubtedly, the peak loads exhibited in this study underestimate the peak loads experienced in impact. To this end, future work is underway to develop an impact testing set up and procedure to better approximate the clinical loading environment.

REFERENCES

[1] W. Dhert, C. Verheyen, L. Braak, J. De Wijn, C. Klein, K. De Groot, and P. Rozing, "A finite element analysis of the push-out test: Influence of test conditions," *Journal of biomedical materials research*, vol. 26, no. 1, pp. 119–130, 1992.

[2] V. C. Mow and R. Huiskes, *Basic orthopaedic biomechanics & mechano-biology*. Lippincott Williams & Wilkins, 2005.

[3] A. C. Stone, "Design and development of a reconfigurable testing system for biomechanical and orthopedic experimental research," Master's thesis, Texas A&M University, 2018.

[4] J. C. Katthagen, M. Schwarze, M. Warnhoff, C. Voigt, C. Hurschler, and H. Lill, "Influence of plate material and screw design on stiffness and ultimate load of locked plating in osteoporotic proximal humeral fractures," *Injury*, vol. 47, no. 3, pp. 617–624, 2016.

[5] J. D. Harris, N. L. Duplantier, R. J. Mitchell, A. Stone, S. Zambrano, D. Delgado, B. S. Lambert, M. R. Moreno, P. C. McCulloch, D. M. Lintner, *et al.*, "A biomechanical comparison of fifth metatarsal jones fracture fixation methods-what is the ideal construct?," *Arthroscopy*, vol. 33, no. 10, p. e82, 2017.

[6] J. D. Wylie, B. Scheiderer, E. Obopilwe, J. B. Baldino, C. Pavano, C. J. Macken, R. Bell, A. D. Mazzocca, R. A. Arciero, and F. B. Imhoff, "The effect of lateral opening wedge distal femoral varus osteotomy on tibiofemoral contact mechanics through knee flexion," *The American journal of sports medicine*, vol. 46, no. 13, pp. 3237–3244, 2018.

[7] J. F. DeLucca, D. Amin, J. M. Peloquin, E. J. Vresilovic, J. J. Costi, and D. M. Elliott, "Off-axis response due to mechanical coupling across all six degrees of freedom in the human disc," *JOR spine*, vol. 2, no. 1, p. e1047, 2019.

[8] J. D. Johnston, M. P. McDonald, and S. A. Kontulainen, "Off-axis loads cause failure of the distal radius at lower magnitudes than axial loads: A side-to-side experimental study,"

Journal of Orthopaedic Research®, vol. 38, no. 8, pp. 1688–1692, 2020.

[9] A. D. Mazzocca, K. J. Burton, A. A. Romeo, S. Santangelo, D. A. Adams, and R. A. Arciero, "Biomechanical evaluation of 4 techniques of distal biceps brachii tendon repair," *The American journal of sports medicine*, vol. 35, no. 2, pp. 252–258, 2007.

[10] M. R. Safran and S. M. Graham, "Distal biceps tendon ruptures: incidence, demographics, and the effect of smoking.," *Clinical Orthopaedics and Related Research (1976-2007)*, vol. 404, pp. 275–283, 2002.

[11] J. G. Seiler III, L. M. Parker, P. D. Chamberland, G. M. Sherbourne, and W. A. Carpenter, "The distal biceps tendon: two potential mechanisms involved in its rupture: arterial supply and mechanical impingement," *Journal of shoulder and elbow surgery*, vol. 4, no. 3, pp. 149–156, 1995.

[12] M. L. Pearl, K. Bessos, and K. Wong, "Strength deficits related to distal biceps tendon rupture and repair: a case report," *American journal of sports medicine*, vol. 26, no. 2, pp. 295–296, 1998.

[13] E. Shields, J. R. Olsen, R. B. Williams, L. Rouse, M. Maloney, and I. Voloshin, "Distal biceps brachii tendon repairs: a single-incision technique using a cortical button with interference screw versus a double-incision technique using suture fixation through bone tunnels," *The American journal of sports medicine*, vol. 43, no. 5, pp. 1072–1076, 2015.

[14] J. E. Hammarstedt, D. D. Savin, and B. A. Goldberg, "Single-incision anatomic repair technique for distal biceps tendon rupture using tunneling device," *Arthroscopy techniques*, vol. 6, no. 4, pp. e945–e950, 2017.

[15] G. C. Berlet, J. A. Johnson, A. D. Milne, S. D. Patterson, and G. J. King, "Distal biceps brachii tendon repair," *The American journal of sports medicine*, vol. 26, no. 3, pp. 428–432, 1998.

[16] D. F. D'Alessandro, C. L. Shields JR, J. E. Tibone, and R. W. Chandler, "Repair of distal biceps tendon ruptures in athletes," *The American journal of sports medicine*, vol. 21, no. 1, pp. 114–119, 1993.

[17] S. E. Lemos, E. Ebramzedeh, and R. S. Kvitne, "A new technique: in vitro suture anchor fixation has superior yield strength to bone tunnel fixation for distal biceps tendon repair," *The American journal of sports medicine*, vol. 32, no. 2, pp. 406–410, 2004.

[18] C. L. Camp, P. B. Voleti, K. T. Corpus, and J. S. Dines, "Single-incision technique for repair of distal biceps tendon avulsions with intramedullary cortical button," *Arthroscopy techniques*, vol. 5, no. 2, pp. e303–e307, 2016.

[19] J. N. Watson, V. M. Moretti, L. Schwindel, and M. R. Hutchinson, "Repair techniques for acute distal biceps tendon ruptures: a systematic review," *JBJS*, vol. 96, no. 24, pp. 2086–2090, 2014.

[20] S. Barnes, S. Coleman, and D. Gilpin, "Repair of avulsed insertion of biceps. a new technique in four cases," *The Journal of bone and joint surgery. British volume*, vol. 75, no. 6, pp. 938–939, 1993.

[21] D. S. Pereira, R. S. Kvitne, M. Liang, F. B. Giacobetti, and E. Ebramzadeh, "Surgical repair of distal biceps tendon ruptures: a biomechanical comparison of two techniques," *The American journal of sports medicine*, vol. 30, no. 3, pp. 432–436, 2002.

[22] J. D. Barlow, R. J. McNeilan, A. Speeckaert, C. T. Beals, and H. M. Awan, "Use of a bicortical button to safely repair the distal biceps in a two-incision approach: a cadaveric analysis," *The Journal of hand surgery*, vol. 42, no. 7, pp. 570–e1, 2017.

[23] I. F. Kodde, R. C. Baerveldt, P. G. Mulder, D. Eygendaal, and M. P. van den Bekerom, "Refixation techniques and approaches for distal biceps tendon ruptures: a systematic review of clinical studies," *Journal of shoulder and elbow surgery*, vol. 25, no. 2, pp. e29–e37, 2016.

[24] D. D. Savin, J. Watson, A. R. Youderian, S. Lee, J. E. Hammarstedt, M. R. Hutchinson, and B. A. Goldberg, "Surgical management of acute distal biceps tendon ruptures," *JBJS*, vol. 99, no. 9, pp. 785–796, 2017.

[25] M. Kettler, J. Lunger, V. Kuhn, W. Mutschler, and M. J. Tingart, "Failure strengths in distal biceps tendon repair," *The American journal of sports medicine*, vol. 35, no. 9, pp. 1544–1548, 2007.

[26] C. R. Mellano, R. M. Frank, J. J. Shin, A. Jain, W. A. Zuke, R. Mascarenhas, E. Shewman, B. J. Cole, A. A. Romeo, N. N. Verma, *et al.*, "Subpectoral biceps tenodesis with peek interference screw: A biomechanical analysis of humeral fracture risk," *Arthroscopy: The Journal of Arthroscopic & Related Surgery*, vol. 34, no. 3, pp. 806–813, 2018.

[27] B. M. Woodall, G. M. Youn, N. Elena, A. Rosinski, M. Chakrabarti, J. Gwosdz, E. C. Shin, N. Pathare, P. J. McGahan, and J. L. Chen, "Anatomic single-incision repair of distal biceps tendon ruptures using intramedullary soft anchors," *Arthroscopy techniques*, vol. 7, no. 11, pp. e1177–e1180, 2018.

[28] G. I. Bain, H. Prem, R. J. Heptinstall, R. Verhellen, and D. Paix, "Repair of distal biceps tendon rupture: a new technique using the endobutton," *Journal of Shoulder and Elbow Surgery*, vol. 9, no. 2, pp. 120–126, 2000.

[29] P. M. Sethi and J. E. Tibone, "Distal biceps repair using cortical button fixation," *Sports medicine and arthroscopy review*, vol. 16, no. 3, pp. 130–135, 2008.

[30] P. Sethi, E. Obopilwe, L. Rincon, S. Miller, and A. Mazzocca, "Biomechanical evaluation of distal biceps reconstruction with cortical button and interference screw fixation," *Journal of shoulder and elbow surgery*, vol. 19, no. 1, pp. 53–57, 2010.

[31] K. R. Sochacki, Z. T. Lawson, R. A. Jack, D. Dong, A. B. Robbins, M. R. Moreno, and P. C. McCulloch, "Distal biceps tendon repair using a double tension slide technique," *Arthroscopy Techniques*, 2020.

[32] M. Jiang, Z. T. Lawson, V. Erel, S. Pervere, T. Nan, A. B. Robbins, A. D. Feed, and M. R. Moreno, “Clamping soft biologic tissues for uniaxial tensile testing: A brief survey of current methods and development of a novel clamping mechanism,” *Journal of the mechanical behavior of biomedical materials*, vol. 103, p. 103503, 2020.

[33] S. H. Naidu, “Interference screw failure in distal biceps endobutton repair: case report,” *The Journal of hand surgery*, vol. 35, no. 9, pp. 1510–1512, 2010.

[34] L. N. Woodard and M. A. Grunlan, “Hydrolytic degradation of pcl–plla semi-ipns exhibiting rapid, tunable degradation,” *ACS biomaterials science & engineering*, vol. 5, no. 2, pp. 498–508, 2018.

[35] J. Black, “" push-out" tests.,” *Journal of biomedical materials research*, vol. 23, no. 11, pp. 1243–1245, 1989.

[36] P. P. Spicer, J. D. Kretlow, S. Young, J. A. Jansen, F. K. Kasper, and A. G. Mikos, “Evaluation of bone regeneration using the rat critical size calvarial defect,” *Nature protocols*, vol. 7, no. 10, pp. 1918–1929, 2012.

[37] J. Kwon, D. J. Lee, M. Kocher, Y.-I. Kim, T.-J. Wu, J. Whitley, and C.-C. Ko, “The inhibition of radial and axial micromovement of bone scaffold with gelfoam® and titanium mesh fixation and its effects on osteointegration,” *Methods and protocols*, vol. 2, no. 1, p. 20, 2019.

[38] M. R. Pfau, K. G. McKinzey, A. A. Roth, L. M. Graul, D. J. Maitland, and M. A. Grunlan, “Shape memory polymer (smp) scaffolds with improved self-fitting properties,” *Journal of Materials Chemistry B*, vol. 9, no. 18, pp. 3826–3837, 2021.

[39] A. S. Arabiyat, M. R. Pfau, M. A. Grunlan, and M. S. Hahn, “Intrinsic osteoinductivity of pcl-da/plla semi-ipn shape memory polymer scaffolds,” *Journal of Biomedical Materials Research Part A*, 2021.

[40] C. Maniatopoulos, J. Sodek, and A. Melcher, “Bone formation in vitro by stromal cells obtained from bone marrow of young adult rats,” *Cell and tissue research*, vol. 254, no. 2, pp. 317–330, 1988.

[41] D. Zhang, O. J. George, K. M. Petersen, A. C. Jimenez-Vergara, M. S. Hahn, and M. A. Grunlan, "A bioactive self-fitting shape memory polymer scaffold with potential to treat cranio-maxillo facial bone defects," *Acta biomaterialia*, vol. 10, no. 11, pp. 4597–4605, 2014.

[42] F. O. Beltran, C. J. Houk, and M. A. Grunlan, "Bioactive siloxane-containing shape-memory polymer (smp) scaffolds with tunable degradation rates," *ACS Biomaterials Science & Engineering*, vol. 7, no. 4, pp. 1631–1639, 2021.

[43] M. R. Pfau, F. O. Beltran, L. N. Woodard, L. K. Dobson, S. B. Gasson, A. Robbins, Z. T. Lawson, W. B. Saunders, M. R. Moreno, and M. A. Grunlan, "Evaluation of a self-fitting, shape memory polymer scaffold in a rabbit calvarial defect model," *Acta Biomaterialia*, 2021.

[44] A. Berner, M. Woodruff, C. Lam, M. Arafat, S. Saifzadeh, R. Steck, J. Ren, M. Nerlich, A. K. Ekaputra, I. Gibson, *et al.*, "Effects of scaffold architecture on cranial bone healing," *International journal of oral and maxillofacial surgery*, vol. 43, no. 4, pp. 506–513, 2014.

[45] T. D. Schiller, "Biomedtrix total hip replacement systems," *Hip Dysplasia, An Issue of Veterinary Clinics of North America: Small Animal Practice, E-Book*, vol. 47, no. 4, p. 899, 2017.

[46] S. Townsend, S. E. Kim, and A. Pozzi, "Effect of stem sizing and position on short-term complications with canine press fit cementless total hip arthroplasty," *Veterinary Surgery*, vol. 46, no. 6, pp. 803–811, 2017.

[47] N. Fitzpatrick, A. Y. Law, M. Bielecki, and S. Girling, "Cementless total hip replacement in 20 juveniles using bfx arthroplasty," *Veterinary Surgery*, vol. 43, no. 6, pp. 715–725, 2014.

[48] E. R. Henderson, A. Wills, A. M. Torrington, A. P. Moores, D. Thomson, G. Arthurs, G. Brown, H. R. Denny, H. W. Scott, I. MacQueen, *et al.*, "Evaluation of variables influencing success and complication rates in canine total hip replacement: results from the british veterinary orthopaedic association canine hip registry (collation of data: 2010–2012)," *Veterinary Record*, vol. 181, no. 1, pp. 18–18, 2017.

[49] J. Fritton, E. Myers, T. Wright, and M. Van Der Meulen, "Loading induces site-specific increases in mineral content assessed by microcomputed tomography of the mouse tibia," *Bone*, vol. 36, no. 6, pp. 1030–1038, 2005.

[50] D. Carter, M. Van der Meulen, and G. Beaupre, "Mechanical factors in bone growth and development," *Bone*, vol. 18, no. 1, pp. S5–S10, 1996.

[51] J. Bätz, P. Messer-Hannemann, F. Lampe, A. Klein, K. Püschel, M. M. Morlock, and G. M. Campbell, "Effect of cavity preparation and bone mineral density on bone-interface densification and bone-implant contact during press-fit implantation of hip stems," *Journal of Orthopaedic Research®*, vol. 37, no. 7, pp. 1580–1589, 2019.

[52] L. Windell, A. Kulkarni, E. Alabort, D. Barba, R. Reed, and H. Singh, "Biomechanical comparison of periprosthetic femoral fracture risk in the exeter v40, cpt, and depuy c-stem in a sawbone model.," *The Journal of Arthroplasty*, 2020.

[53] J. Elfar, S. Stanbury, R. M. G. Menorca, and J. D. Reed, "Composite bone models in orthopaedic surgery research and education," *The Journal of the American Academy of Orthopaedic Surgeons*, vol. 22, no. 2, p. 111, 2014.

[54] M. Collier, P. Noble, J. Alexander, and L. Miller, "The effect of cutting tooth design on the machining capability of femoral broaches," in *TRANSACTIONS OF THE ANNUAL MEETING-ORTHOPAEDIC RESEARCH SOCIETY*, pp. 417–417, ORTHOPAEDIC RESEARCH SCOIETY, 1996.

[55] H. A. Kishawy, A. Hosseini, B. Moetakef-Imani, and V. P. Astakhov, "An energy based analysis of broaching operation: Cutting forces and resultant surface integrity," *CIRP annals*, vol. 61, no. 1, pp. 107–110, 2012.

[56] E. C. Ozelkan, O. Ozturk, and E. Budak, "Identifying parameters of a broaching design using non-linear optimisation," *International Journal of Modelling, Identification and Control*, vol. 12, no. 3, pp. 244–252, 2011.

[57] O. Ozturk and E. Budak, "Modeling of broaching process for improved tool design," in *ASME International Mechanical Engineering Congress and Exposition*, vol. 37203, pp. 291–300, 2003.

[58] A. Hosseini and H. Kishawy, "Prediction of cutting forces in broaching operation," *Journal of Advanced Manufacturing Systems*, vol. 12, no. 01, pp. 1–14, 2013.

[59] J.-T. Hausmann, "Sawbones in biomechanical settings-a review," *Osteosynthesis and Trauma Care*, vol. 14, no. 04, pp. 259–264, 2006.

[60] M. Poukalova, C. M. Yakacki, R. E. Guldberg, A. Lin, M. Saing, S. D. Gillogly, and K. Gall, "Pullout strength of suture anchors: effect of mechanical properties of trabecular bone," *Journal of biomechanics*, vol. 43, no. 6, pp. 1138–1145, 2010.

[61] A. Kinaci, V. Neuhaus, and D. C. Ring, "Trends in bone graft use in the united states," *Orthopedics*, vol. 37, no. 9, pp. e783–e788, 2014.

[62] J. D. Boerckel, Y. M. Kolambkar, H. Y. Stevens, A. S. Lin, K. M. Dupont, and R. E. Guldberg, "Effects of in vivo mechanical loading on large bone defect regeneration," *Journal of Orthopaedic Research*, vol. 30, no. 7, pp. 1067–1075, 2012.

[63] K. S. Stakleff, F. Lin, L. A. S. Callahan, M. B. Wade, A. Esterle, J. Miller, M. Graham, and M. L. Becker, "Resorbable, amino acid-based poly (ester urea) s crosslinked with osteogenic growth peptide with enhanced mechanical properties and bioactivity," *Acta Biomaterialia*, vol. 9, no. 2, pp. 5132–5142, 2013.

APPENDIX A

MATERIALS AND WORK INSTRUCTIONS FOR PUSH-OUT TESTING

A.1 BILL OF MATERIALS

- Custom 3D printed clamp (available for download)
- Custom 3D printed position aligner (available for download)
- 2-56 x ¡" hex head screw, 18-8 stainless steel (McMaster 92314A404), QTY:1
- 2-56 hex nut, 18-8 stainless steel (McMaster 91841A003), QTY: 1
- 2-56 x " socket head screw, 18-8 stainless steel (McMaster 92196A086), QTY: 2
- 2-56 flanged knurled-head thumb nut, 18-8 stainless steel (McMaster 95150A110), QTY: 2
- 5 mm diameter stainless steel push-out rod (bilateral murine samples)
- 8 mm diameter stainless steel push-out rod (leporine samples and unilateral murine samples)
- Load cell (Futek LSB 210, 100lbf capacity)
- 1 L of 0.1 M PBS solution at Room Temperature
- Newport M-461 xyz linear stage
- Aluminum base block with slot
- 8020 aluminum extrusions

A.2 WORK INSTRUCTIONS

1. Assemble testing clamp (Figure 4).
   (a) Print one (1) clamp per test sample.

(b) Place the 2-56 hex head screw through the slotted hinge of the clamp and secure with the 2-56 thread hex nut.

(c) Place the long 2-56 socket head screws through the bottom of the clamp such that the threaded end is coming out through the top.

(d) Loosely screw on the knurled knobs onto the socket head screws.

2. Set up testing fixture

(a) Initialize testing machine, attach load cell, and configure for testing.

(b) Mount the push-out rod on the load cell.

(c) Mount the 3D printed alignment tool to the push-out rod.

(d) Assemble the 8020 extrusions and aluminum block to the Newport linear stage; mount assembly to the testing machine with the aluminum block centered approximately 10 mm under the push-out rod.

(e) Place an assembled 3D printed clamp into the aluminum block.

(f) Adjust the linear stage until the targeted notch of the clamp and push-out rod alignment tool are mated (A.1).

3. Prepare the testing samples

(a) Take the explanted calvarium and slide it into an assembled clamp with the concave side of the calvarium facing up.

(b) Shine a bright light through the bottom of the clamp to illuminate the boundary of the defect ().

(c) Position the explanted calvarium such that the entirety of the defect is within the boundary of the through hole (Figure 6).

(d) Tighten the knurled knobs with your thumb until the sample is secured in place. If the top clamp begins to bend, then the knobs are getting too tight.

(e) Store the assembled test article in the PBS solution until it is time to test.

4. Performing experiment

(a) Remove the assembled test article from the PBS bath and secure it in the slot of the aluminum block.

(b) Verify the clamp is aligned with the push-out rod aligner then remove the push-out aligner (Figure 8).

(c) Bring the actuator down until the push-out rod registers 5 N of preload, then zero displacement.

(d) Proceed with the experiment, displacing the push-out rod at 5 mm/min (0.0083 mm/s) to twice the thickness of the sample to ensure the rod has fully pushed through (Figure 9).

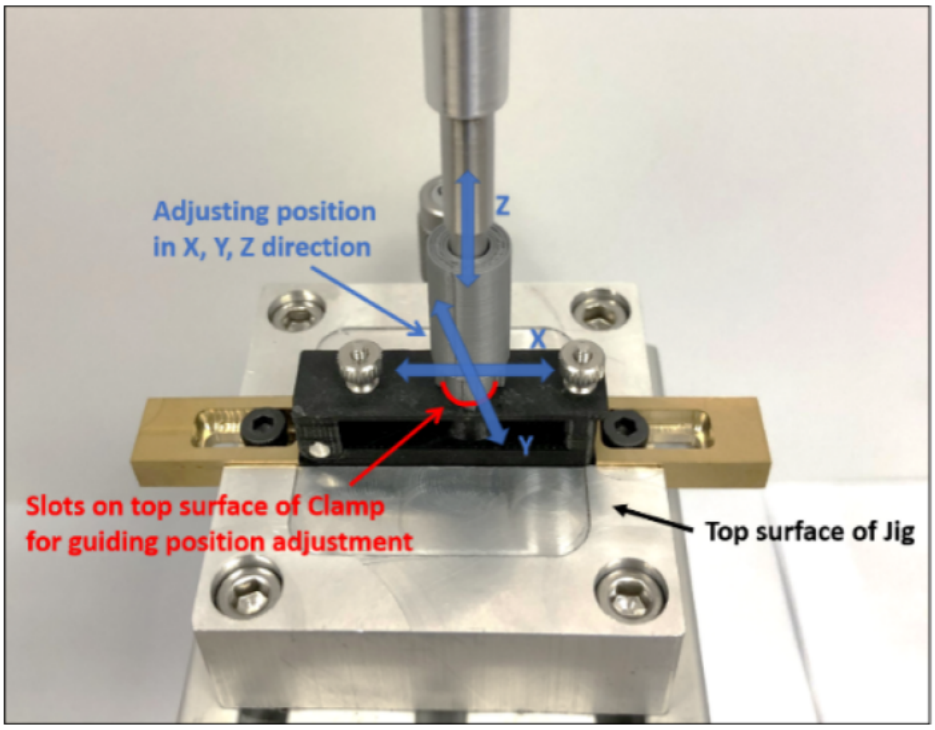

Figure A.1: Alignment of the push-out rod with the through-hole by mating the targeted notch patterns.

APPENDIX B

BIOMECHANICAL EVALUATION OF JOINT STABILITY IN REPAIRED HIP CAPSULOTOMY

Acknowledgements: Houston Methodist Research Hospital, Cris Mathew, Joshua D. Harris. This project was a team effort for the BMEL and I would like to acknowledge the contributions of Aaron Stone, Andrew Robbins, Raghuveer Lalitha Sridhar, Shannon Ingram, and the army of undergraduates that had a hand in this project. Special thanks to my undergraduate assistants Douglas Fuller, Laura Homiller, and Ryan Walford who went above and beyond in assisting with these experiments.

B.1 INTRODUCTION

Femoroacetabular impingement (FAI) is a condition caused by excessive bony development of either or both the acetabulum or proximal femoral head neck junction that causes abnormal kinematics of the joint resulting in labral or chondral damage. This damage can lead to degeneration and arthritis. Recent developments have led to advanced instrumentation and techniques that allow for improved osseous correction and soft tissue repair. When entering the joint, capsulotomies are made to increase exposure and access into the joint and improve visualization along the proximal femur. Although this vital structure is lacerated during exposure, there is limited evidence on the importance of its closure and the effects on hip mechanics and stability. This study was designed to establish a baseline mechanical stability of the hip and evaluate the effects from an interportal capsulotomy, T-capsulotomy, with repairs and a complete capsulectomy.

B.2 METHODS

Five fresh-frozen cadavers from T12 vertebra to the distal end of the femurs were dissected to remove all soft tissue with little to no influence on the mechanics of the hip joint. Each cadaver was cut from the sacroiliac junction through the pubic symphysis to produce 10 paired hip

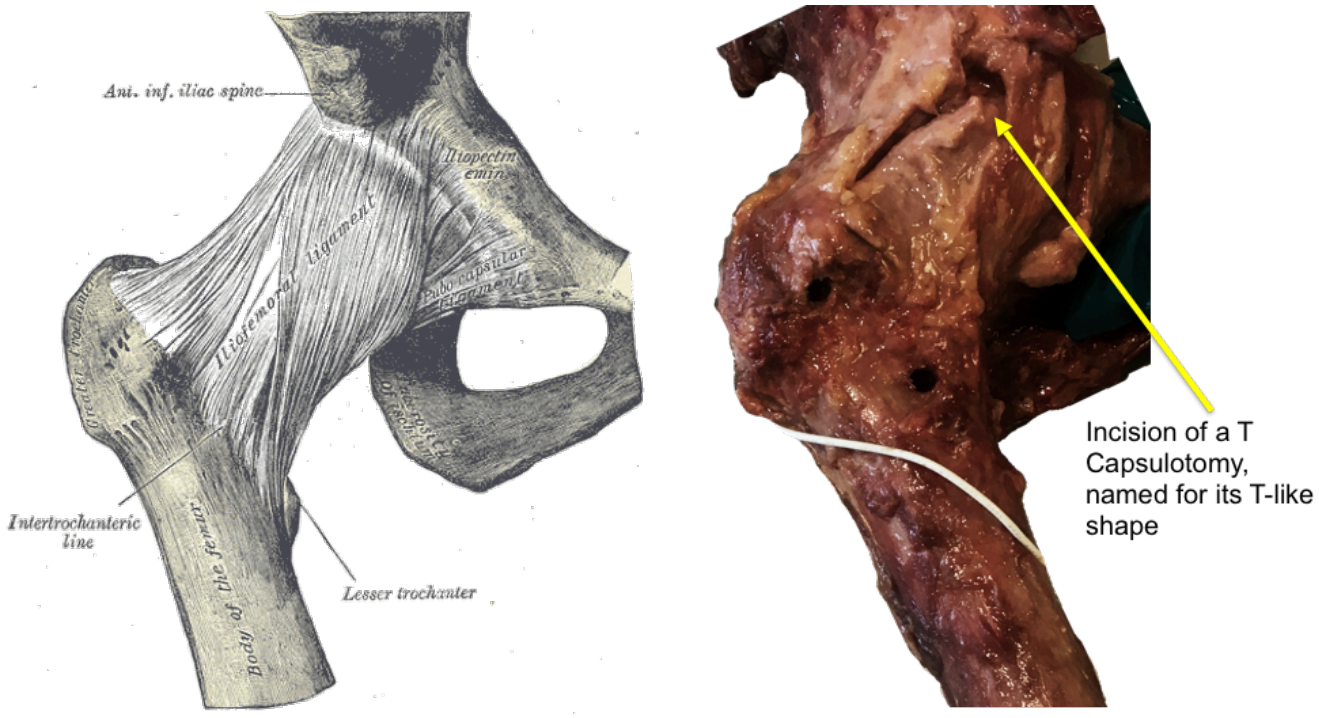

Figure B.1: Left: Illustration hip joint capsule[3]. Right: Hip joint after undergoing T Capsulotomy

samples. Each hip sample was attached to a custom biomechanical load frame and adjusted to 4 configurations: physiological neutral, 10°abduction, 45°flexion, and "perpendicular": a simulation of the clinical joint stability evaluation wherein the loading line is perpendicular to the acetabulum. For each configuration, the femur was distracted along the physiologically loading line at 1 mm/s until either reaching 400 N or 15 mm, conditions deemed to be damaging to the tissue. Maximum extension was kept constant for each sample. Following baseline evaluation, the mechanical testing regiment was repeated for each hip following Inter-Portal Capsulotomy, T Capsulotomy, Partial Repair (or single repair), and Full Repair (or double repair). The datapoint of interest was the maximum load achieved prior to failure of the suction seal (Fig B.5). The average peak load for each condition was normalized to the average peak load of the baseline; ANOVA with Tukey post-hoc was used to calculate statistical significance.

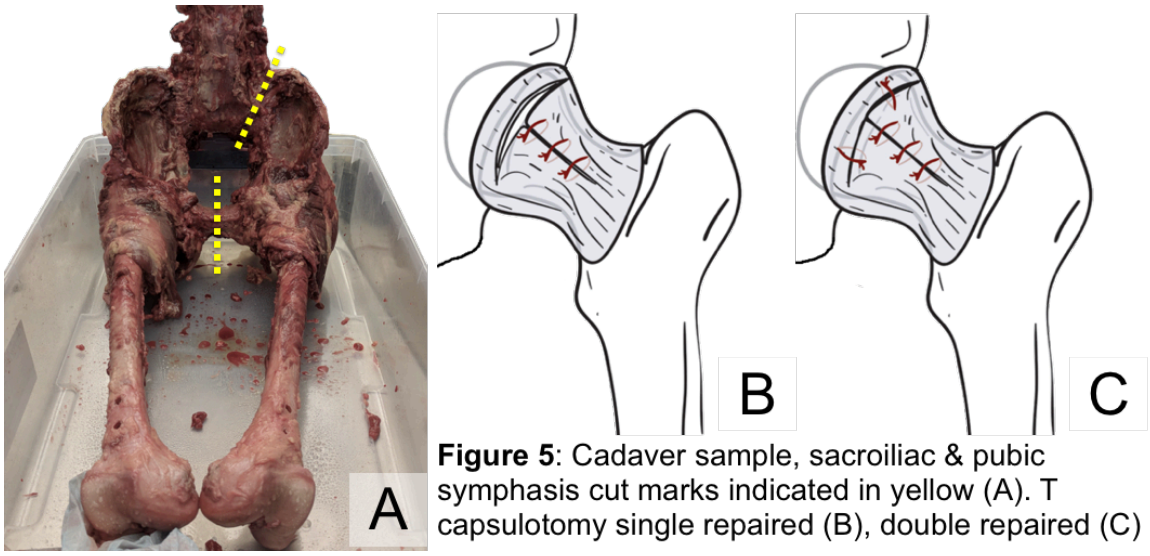

Figure 5: Cadaver sample, sacroiliac & pubic symphasis cut marks indicated in yellow (A). T capsulotomy single repaired (B), double repaired (C)

Figure B.2: Cadaver sample, sacroiliac and pubic symphasis cut marks indicated in yellow (A). T capsulotomy single repaired (B), double repaired (C).

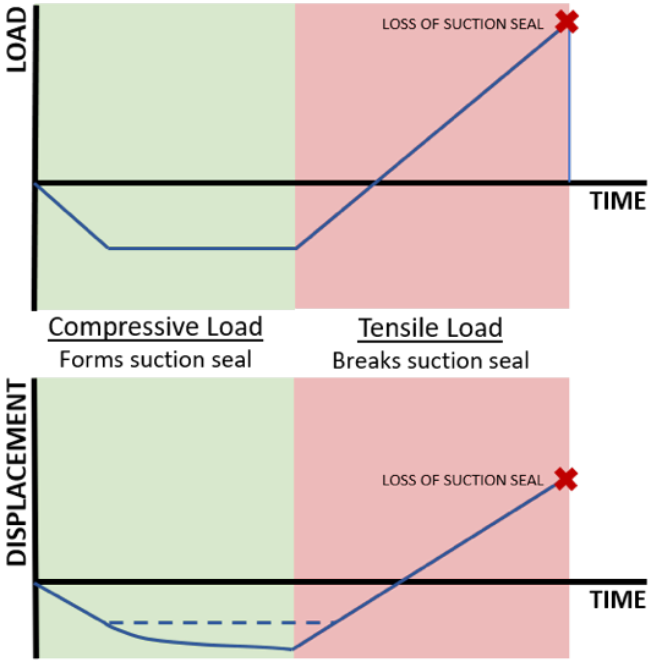

Figure B.3: Graphical representation of input parameters and idealized sample response.

B.3 RESULTS

Five hip samples were selected for analysis in the 10°abduction geometry. Compared to the baseline, force required to rupture the suction seal for the IP capsulotomy was not significantly different ($p = 0.117$); however, force was significantly lower than the baseline in all other conditions ($p < 0.05$). Post-hoc analysis showed no significant difference between the various non-baseline conditions compared to each other.

B.4 DISCUSSION

The load at which the suction seal broke was compared across all conditions and normalized relative to the baseline. No significant difference in the suction seal strength was found between the repaired and unrepaired conditions. Thus, based on these data it is unclear whether capsulotomy repairs return stability to the hip joint. There are significant limitations to these results as the data represents only the 10°abduction configuration. All of the hips in this study were FAI positive; however, in comparable studies, FAI was considered an exclusion criterion. This study was conducted in air, whereas the hip suction seal is formed with the aid of water pressurization. These experimental design flaws severely limit the application of this study beyond a validation of the R.T.S. versatility. Being able to perform a large scale cadaveric study of this nature would have been enormously difficult to do on a standard testing machine.

Figure B.4: Hip sample loaded in reconfigurable testing machine

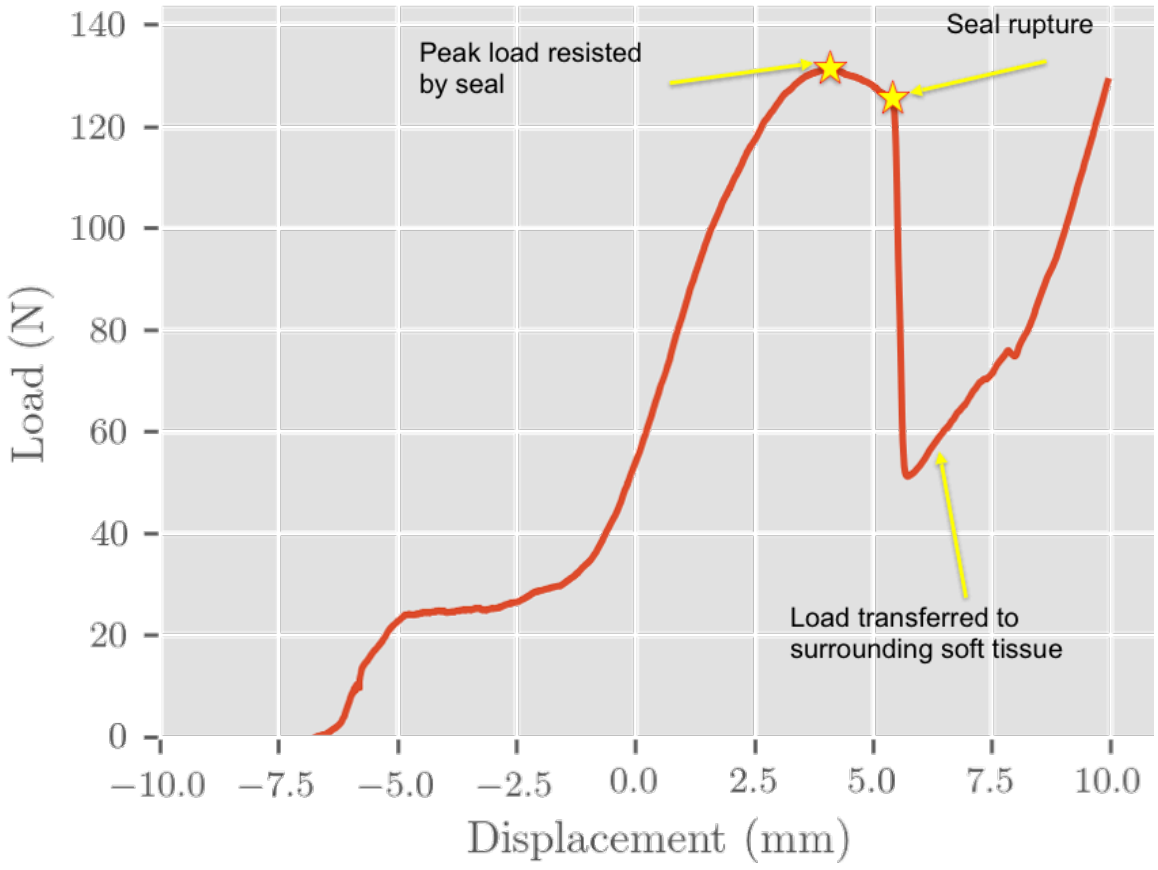

Figure B.5: Typical force extension chart in response to femoral distraction. Sharp load drop-off is indicative of the seal breaking. The peak load prior to seal rupture is the point of interest.

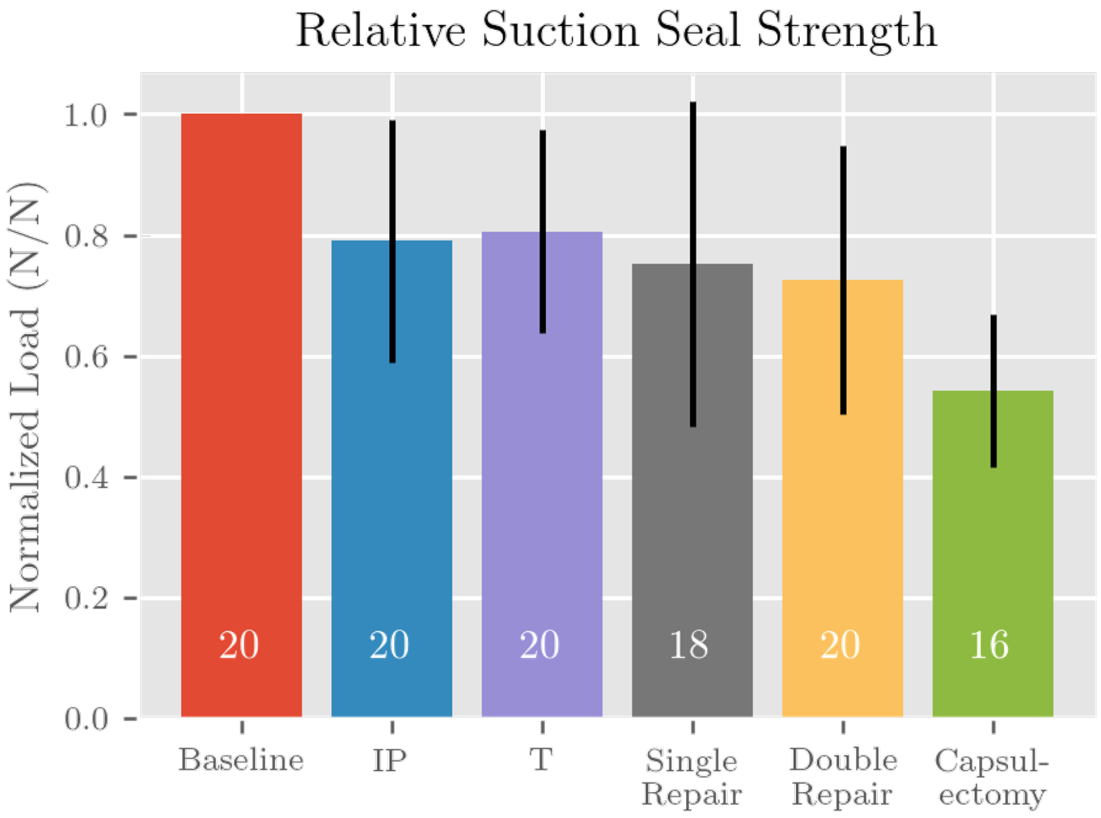

Figure B.6: Suction seal loads across five hips in 10°abduction; loads are normalized relative to the baseline suction seal strength. White numbers indicate the number of trials

APPENDIX C

FRACTURE DEVELOPMENT IN A BIODEGRADABLE CYLINDRICAL BONE FIXATION DEVICE AFTER DEGRADATION

Acknowledgments: This section was co-written with Raghuveer Lalitha Sridhar. My contributions are to the methods development, data analysis, and updated conclusion. Special thanks to my undergraduate assistant, Andra Thurtell, who assisted in conducting the experiments and collating the data. The discussion here is preliminary as we are continuing to analyze this data.

C.1 INTRODUCTION

Between 1992 and 2007, almost 2 million patients in the United States received surgical bone grafts [61]. However, surgical autografting of bone defects has significant limitations[[62]. There is a pressing need for a biodegradable implant that promotes bone regeneration in critical size defects while also providing the mechanical stability required during the healing period. Highly comminuted fractures are clinically challenging and often require metallic bone plates for fixation and support. Unfortunately, these plates restore function but do not aid healing and sometimes result in non-union of the bones. A load bearing fracture fixation device consisting of a biodegradable polymer tube, manufactured from poly-(ester urea) (PEU) [63] has been designed to support critical size defects in long bones during recovery after a comminuted fracture and ultimately lead to healing. While it is important that the device be biodegradable to preclude the need for secondary surgery once the defect has been healed, it is crucial that the degradation experienced by the device inside the body does not compromise its mechanical strength before bone strength is sufficiently restored. It is therefore desirable to subject the device to degradation in vitro to study the effects on its mechanical performance. In this study, these devices are subjected to short term degradation and the effects on failure strength and fracture development are investigated.

C.2 METHODS

In this study, the fixation devices are tested under a 4-point bending configuration to simulate a worst-case-scenario mechanical load in the ovine animal model. Twelve PEU shells were tested under two conditions: dry (5 shells) or 1 hr degradation (7 shells). For the dry condition, sterile, injection molded devices were removed from their packaging, photographed and subjected to 4-point bending to failure (4 lever arm with a bending rate of approximately 24 deg/s). For the 1 hr degradation condition, devices were subjected to a static bending load of 200 inůlbf of bending torque in a saline bath at 37 degree C for 1 hour, prior to 4-point bend testing to failure. Following the test to failure, the shells were reconstructed and photographed, and the fracture patterns were qualitatively characterized. Eleven (11) PEU shells were placed into a degradation bath; two were excluded due to immediate failure, leaving nine (9) at a time point of 7 days (n=4) or 14 days (n=5). Conditions of the bath were 37žC, nominal, with phosphate-buffered saline at 7.4 buffered pH. Prior to immersion, the length, diameter, and mass was measured for each shell. All sides of the shells were photographed, placed on FIX-0037, and then loaded. Loading conditions were, nominally, 20 lbf applied on a 10 inch lever arm to produce a 200 in*lbf bending moment. The angle of the pin blocks were measured repeatedly for the indicated time length or until a failure condition was met. Failure was either when the shell fractured or the load contacted the table at a pin block angle of nominally 30 degrees. After either failure or reaching the specified time point, the shells were removed from the bath, photographed, and stored. Ten (10) shells were placed into the degradation bath at time point t = 7 days. Conditions of the bath were 37°C, nominal, with phosphate-buffered saline at 7.4 buffered pH. Prior to immersion, the length, diameter, and mass was measured for each shell. After the 1 week time point, they were removed, photographed before testing, and tested to failure using the WINS-0005 instructions on four-point bending to failure. After testing, the fragments were collected and the shells were reconstructed using glue and then photographed. The reconstructed photographs were used to determine the fracture type of the tested shell. There were 4 possible fracture types: Type 0 - no fracture, Type I - 1 chip, Type II - a main chip with additional cracking, Type III - a complicated network of chips and cracking.

Welchs t-tests were used to analyze statistical differences in failure torques (calculated as failure load multiplied by the length of the lever arm) between the Type III and combined groups Type I and II, as well as between the degraded and dry groups.

C.3 RESULTS

An exponential curve was fit to the data for each shell in the form $d = Ce^{mt}$ where d is the angular displacement in degrees, C is the initial angle in degrees, e is Eulers number, m is a time coefficient, and t is time in hours. The average value for C = 3.495 $\pm$ 0.503 (SD) deg and m = 0.0105 $\pm$ 0.0015 (SD). The average torque at failure was 176.84 N*m ($\pm$82.32 N*m) SD. Samples which showed brittle failure exhibited a stiffness of 456.19 N/mm $\pm$ 1.74 N/mm SD whereas samples with Type 0 failure exhibited a stiffness of 489.02 N/mm $\pm$ 16.44 N/mm.

C.4 DISCUSSION

High standard deviations have been observed in the failure strengths of the specimens tested, suggesting that the manufacturing process might be introducing too much variability into the specimens. A larger sample size is needed to make statistically relevant inferences about failure torques between the dry and degraded groups (p=.50). When the shells are grouped based on the fracture type, it can be seen that the dry samples failed predominantly as a Type III fracture, while the degraded samples were more likely to fail with a Type I or Type II fracture pattern. A statistically significant difference in strength was observed between Type III and Types I ,II (p=.034), with the Type III fractures occurring at higher failure loads. This suggests that the degradation process has an effect on the structural integrity of the shell, causing a simpler fracture pattern and failure at lower loads.

C.5 CONCLUSION

The shells demonstrated a creep-like behavior in the bath, suggesting they become more ductile in exposure to heat and water. The device in its current form will not suffice as a fracture fixation device, in part due to the low strength which would lead to fracture failure in the early postoperative period. Secondarily, if the device were to initially survive, the increased ductility

suggests deformation failure (i.e. failure by deforming > 30°) would be expected within 10 days from normal standing use. That is insufficient time for a callus to form.